ISSN 8755-6839

SCIENCE OF TSUNAMI HAZARDS

The International Journal of The Tsunami Society

Volume 20 Number 5 Published Electronically 2002

THE TSUNAMI SOCIETY
P. O. Box 37970,
Honolulu, HI 96817, USA

WWW.STHJOURNAL.ORG

OBJECTIVE: **The Tsunami Society** publishes this journal to increase and disseminate knowledge about tsunamis and their hazards.

DISCLAIMER: Although these articles have been technically reviewed by peers, **The Tsunami Society** is not responsible for the veracity of any statement, opinion or consequences.

Submit manuscripts of articles, notes or letters to the Editor. If an article is accepted for publication the author(s) must submit a scan ready manuscript, a TeX or a PDF file in the journal format. Issues of the journal are published electronically in PDF format. The journal issues for 2002 are available at

http://www.sthjournal.org.

Tsunami Society members will be advised by e-mail when a new issue is available and the address for access. There are no page charges or reprints for authors.

Previous volumes of the journal are available in PDF format at

http://epubs.lanl.gov/tsunami/

and on a CD-ROM from the Society to Tsunami Society members.

ISSN 8755-6839 **http://www.sthjournal.org**

Published Electronically by The Tsunami Society in Honolulu, Hawaii, USA

.

MODELING THE 1958 LITUYA BAY MEGA-TSUNAMI, II

Charles L. Mader
Los Alamos National Laboratory
Los Alamos, NM 87545 U.S.A.
Michael L. Gittings
Science Applications International Corporation
Los Alamos, NM 87545 U.S.A.
LA-UR-02-5632

ABSTRACT

Lituya Bay, Alaska is a T-Shaped bay, 7 miles long and up to 2 miles wide. The two arms at the head of the bay, Gilbert and Crillon Inlets, are part of a trench along the Fairweather Fault. On July 8, 1958, an 7.5 Magnitude earthquake occurred along the Fairweather fault with an epicenter near Lituya Bay.

A mega-tsunami wave was generated that washed out trees to a maximum altitude of 520 meters at the entrance of Gilbert Inlet. Much of the rest of the shoreline of the Bay was denuded by the tsunami from 30 to 200 meters altitude.

In the previous study it was determined that if the 520 meter high run-up was 50 to 100 meters thick, the observed inundation in the rest of Lituya Bay could be numerically reproduced. It was also concluded that further studies would require full Navier-Stokes modeling similar to those required for asteroid generated tsunami waves.

During the Summer of 2000, Hermann Fritz conducted experiments that reproduced the Lituya Bay 1958 event. The laboratory experiments indicated that the 1958 Lituya Bay 524 meter run-up on the spur ridge of Gilbert Inlet could be caused by a landslide impact.

The Lituya Bay impact landslide generated tsunami was modeled with the full Navier-Stokes AMR Eulerian compressible hydrodynamic code called SAGE with includes the effect of gravity.

INTRODUCTION

Lituya Bay, Alaska is on the northeast shore of the Gulf of Alaska. It is an ice-scoured tidal inlet with a maximum depth of 220 meters and a narrow entrance with a depth of only 10 meters. It is a T-Shaped bay, 7 miles long and up to 2 miles wide. The two arms at the head of the bay, Gilbert and Crillon Inlets, are part of a trench along the Fairweather Fault. On July 8, 1958, a 7.5 Magnitude earthquake occurred along the Fairweather fault with an epicenter near Lituya Bay.

A mega-tsunami wave was generated that washed out trees to a maximum altitude of 520 meters at the entrance of Gilbert Inlet. Much of the rest of the shoreline of the Bay was denuded by the tsunami from 30 to 200 meters altitude.

During the last 150 years 5 giant waves have occurred in Lituya. The previous event occurred on October 27, 1936 which washed out trees to a maximum altitude of 150 meters and was not associated with an earthquake.

Don Miller recorded all that was known in 1960 about the giant waves in Lituya bay in reference 1.

The July 9, 1958 earthquake occured at about 10:15 p.m. which is still daylight at Lituya Bay. The weather was clear and the tide was ebbing at about plus 5 feet. Bill and Vivian Swanson were on their boat anchored in Anchorage Cove near the western side of the entrance of Lituya Bay. Their astounding observations are recorded in reference 2 and were as follows:

"With the first jolt, I tumbled out of the bunk and looked toward the head of the bay where all the noise was coming from. The mountains were shaking something awful, with slide of rock and snow, but what I noticed mostly was the glacier, the north glacier, the one they call Lituya Glacier.

I know you can't ordinarily see that glacier from where I was anchored. People shake their heads when I tell them I saw it that night. I can't help it if they don't believe me. I know the glacier is hidden by the point when you're in Anchorage Cove, but I know what I saw that night, too.

The glacier had risen in the air and moved forward so it was in sight. It must have risen several hundred feet. I don't mean it was just hanging in the air. It seems to be solid, but it was jumping and shaking like crazy. Big chunks of ice were falling off the face of it and down into the water. That was six miles away and they still looked like big chunks. They came off the glacier like a big load of rocks spilling out of a dump truck. That went on for a little while – its hard to tell just how long – and then suddenly the glacier dropped back out of sight and there was a big wall of water going over the point. The wave started for us right after that and I was too busy to tell what else was happening up there."

A 15 meter high wave rushed out of the head of the bay toward Swanson's anchored boat. The boat shot upward on the crest of the wave and over the tops of standing spruce trees on the entrance spit of Lituya Bay. Swanson looked down on the trees growing on the spit and said he was more than 25 meters above their tops. The wave crest broke just outside the spit and the boat hit bottom and foundered some distance from the shore. Swanson saw water pouring over the spit, carrying logs and other debris. The Swansons escaped in their skiff to be picked up by another fishing boat 2 hours later.

The front of Lituya Glacier on July 10 was a nearly straight, vertical wall almost normal to the trend of the valley. Comparisions with photographs of the glacier taken July 7 indicate that 400 meters of ice had been sheared off of the glacier front (reference 1).

After the earthquake there was a fresh scar on the northeast wall of Gilbert Inlet, marking the recent position of a large mass of rock that had plunged down the steep slope into the water. The next day after the earthquake and tsunami, loose rock debris on the fresh scar was still moving at some places, and small masses of rock still were falling from the rock cliffs near the head of the scar. The dimensions of the slide on the slope are accurate but the thickness of the slide mass normal to the slope can only be estimated. The main mass of the slide was a prism of rock that was 730 meters and 900 meters along the slope with a maximum thickness of 90 meters and average thickness of 45 meters normal to the slope, and a center of gravity at about 600 meters altitude. As described in reference 1 this results in an approximate volume of 30 million cubic meters (40 million cubic yards).

Miller in reference 1 concluded that "the rockslide was the major, if not the sole cause of the 1958 giant wave." The Swanson observations have not been believed as they indicate that a lot more than a simple landslide occurred.

Shallow Water Modeling

In reference 3 shallow water modeling was performed using the *SWAN* non-linear shallow water code which includes Coriolis and frictional effects. The *SWAN* code is described in reference 4. The generation and propagation of the tsunami wave of July 8, 1958 in Lituya Bay was modeled using a 92.75 by 92.75 meter grid of the topography. The 3 by 6 second land topography was generated from the Rocky Mountain Communication's CD-ROM compilation of the Defense Mapping Agency (DMA) 1 x 1 degree blocks of 3 arc second elevation data. The sea floor topography was taken from sea floor topographic maps published in reference 1. The grid was 150 by 150 cells and the time step was 0.15 second.

It was concluded that the amount of water displaced by a simple landslide or an earthquake along the Fairweather fault at the head of the bay is insufficient to cause the observed tsunami wave. The water in the glacial lake is a possible source of the large volume of water required but no mechanism is known that would result in the observed 520 meter inundation.

The Swanson observations suggest a water wave lifted the front of the glacier up and moved it out from its initial position and generated the 520 meter high wave run-up.

George Pararas-Caryannis suggested that the wave was formed by a landslide impact similar to an asteroid impact, making a cavity in the inlet ocean to the depth of the inlet floor (120 meters) near the landslide.

The water in the inlet with the width of the landslide and between the landslide and the 520 meter high run-up is sufficient to cover the run-up region to 100 meter height. In reference 3 it was shown that this high water layer is sufficient to form a wave that will reproduce the observed flooding of the bay beyond the inlet.

It was concluded that the P.C. landslide impact model would require full Navier-Stokes modeling similar to that required for asteroid generated waves. In 1999 it appeared that the numerical technology required would not become available for many decades.

Physical Modeling

During the Summer of 2000, Hermann Fritz conducted experiments that reproduced the Lituya Bay 1958 event. A 1:675 scale laboratory model of Lituya Bay was built at VAW at the Swiss Federal Institute of Technology at Zurich, Switzerland. The laboratory experiments indicated that the 1958 Lituya Bay 524 meter run-up on the spur ridge of Gilbert Inlet could be caused by a landslide impact. The study was reported in reference 5. A novel pneumatic landslide generator was used to generate a high-speed granular slide with a controlled impact velocity and shape. A granular slide with the density and volume given by Miller in reference 1 impacted with a mean velocity of 110 m/s. It generated a large air cavity and an extremely nonlinear wave with a maximum height of about 160 meters which ran up to an elevation of 530 meters above mean sea level.

COMPRESSIBLE NAVIER STOKES MODELING

The Lituya Bay impact landslide generated tsunami was modeled with the recently developed full Navier-Stokes AMR (Automatic Mesh Refinement) Eulerian compressible hydrodynamic code called SAGE (6, 7, 8, 9) which includes the effects of gravity.

The initial geometry reproduced that used by Fritz in his physical experimental modeling in reference 4 and is shown in Figure 1.

The calculated density profiles are shown in Figure 2 for a rockslide moving with a resultant velocity of 110 meters/second (X and Y component velocities of 77.8 meters/sec). The rockslide had an area of 21,000 square meters and was basalt with a density of 2.868 g/cc. The initial water depth was 120 meters and the length was 1.4 km. The calculated maximum wave height in the bay was about 250 meters above sea level which ran up to 580 meters which is to be compared to the observed 524 meters.

The computer animation is available in the file litavi.zip at
http://t14web.lanl.gov/Staff/clm/tsunami.mve/tsunami.htm
under the hyperlink “Lituya Impact Landslide”.

CONCLUSIONS

The mega-tsunami that occurred on July 8, 1958 in Lituya Bay washed out trees to a maximum altitude of 520 meters at the entrance of Gilbert Inlet. Much of the rest of the shoreline of the Bay was denuded by the tsunami from 30 to 200 meters altitude.

The Lituya Bay impact generated tsunami was modeled with the full Navier-Stokes AMR Eulerian compressible hydrodynamic code called SAGE. The capability now exists to evaluate the potential impact landslide tsunami hazards for vunerable regions of the world.

Los Alamos National Laboratory Contribution LA-UR-02-5632

REFERENCES

1. Don J. Miller, "Giant Waves in Lituya Bay, Alaska" Geological Survey Professional Paper 354-C, U. S. Government Printing Office, Washington (1960).
2. Frances E. Calwell, **Land of The Ocean Mists-The Wild Ocean Coast West of Glacier Bay**, Alaska Northwest Publishing Company, Edmonds, Washington ISBN 0-88240-311-7 (1986).
3. Charles L. Mader, "Modeling the 1958 Lituya Bay Tsunami", Science of Tsunami Hazards, Volume 17, Number 1, pages 57-67.(1999).
4. Charles L. Mader, **Numerical Modeling of Water Waves,** University of California Press, Berkeley, California (1988).
5. Hermann M. Fritz, Willi H. Hager and Hans-Erwin Minor, "Lituya Bay Case: Rockslide Impact and Wave Runup", Science of Tsunami Hazards, Volume 19, Number 1, pages 3-22 (2001).
6. M. L. Gittings, "1992 SAIC's Adaptive Grid Eulerian Code", Defense Nuclear Agency Numerical Methods Symposium, 28-30 (1992).
7. R. L. Holmes, G. Dimonte, B. Fryxell, M. L. Gittings, J. W. Grove, M. Schneider, D. H. Sharp, A. L. Velikovich, R. P. Weaver and Q. Zhang, "Richtmyer-Meshkov Instability Growth: Experiment, Simulation and Theory", J. Fluid Mech. 389, 55-79 (1999).
8. R. M. Baltrusaitis, M. L. Gittings, R. P. Weaver, R. F. Benjamin and J. M. Budzinski, "Simulation of Shock-Generated Instabilities," Phys. Fluids, 8, 2471-2483 (1996).
9. Charles L. Mader, John D. Zumbro and Eric N. Ferm, "Proton Radiographic and Numerical Modelng of Colliding Diverging PBX-9502 Detonations," Twelfth International Symposium on Detonation, August 11-16, 2002, San Diego, California. Also at http://t14web.lanl.gov/Staff/clm/prad77/prad77.htm.

Figure 1

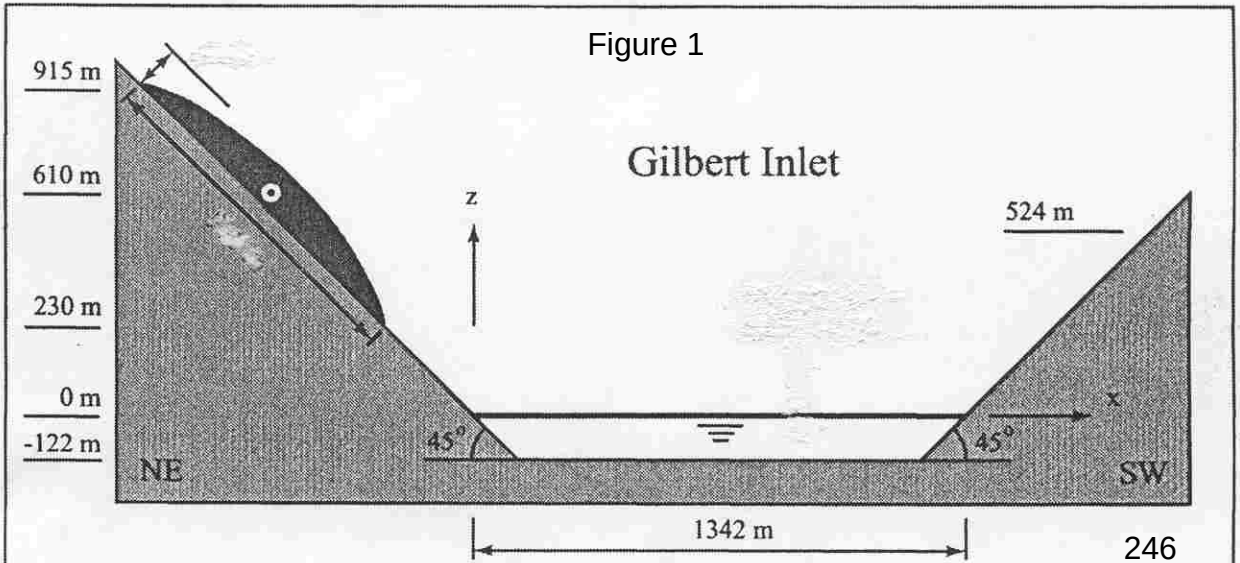

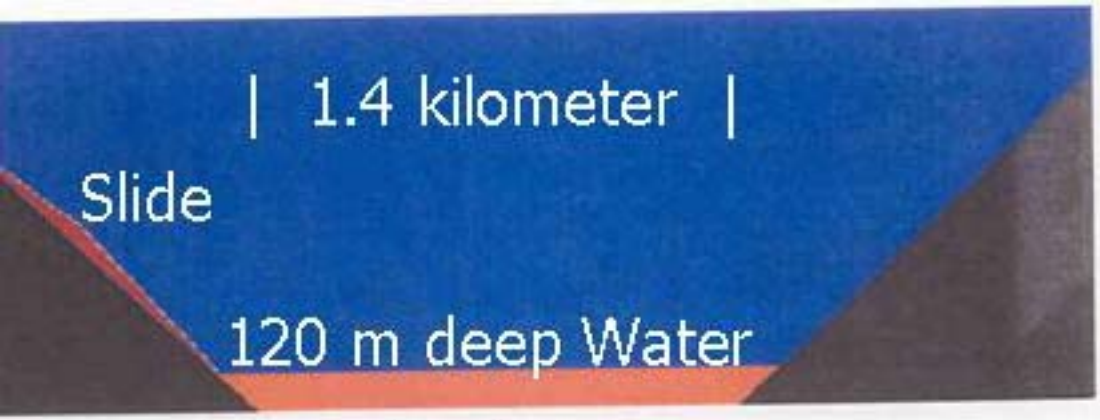

Figure 2 Density Profiles

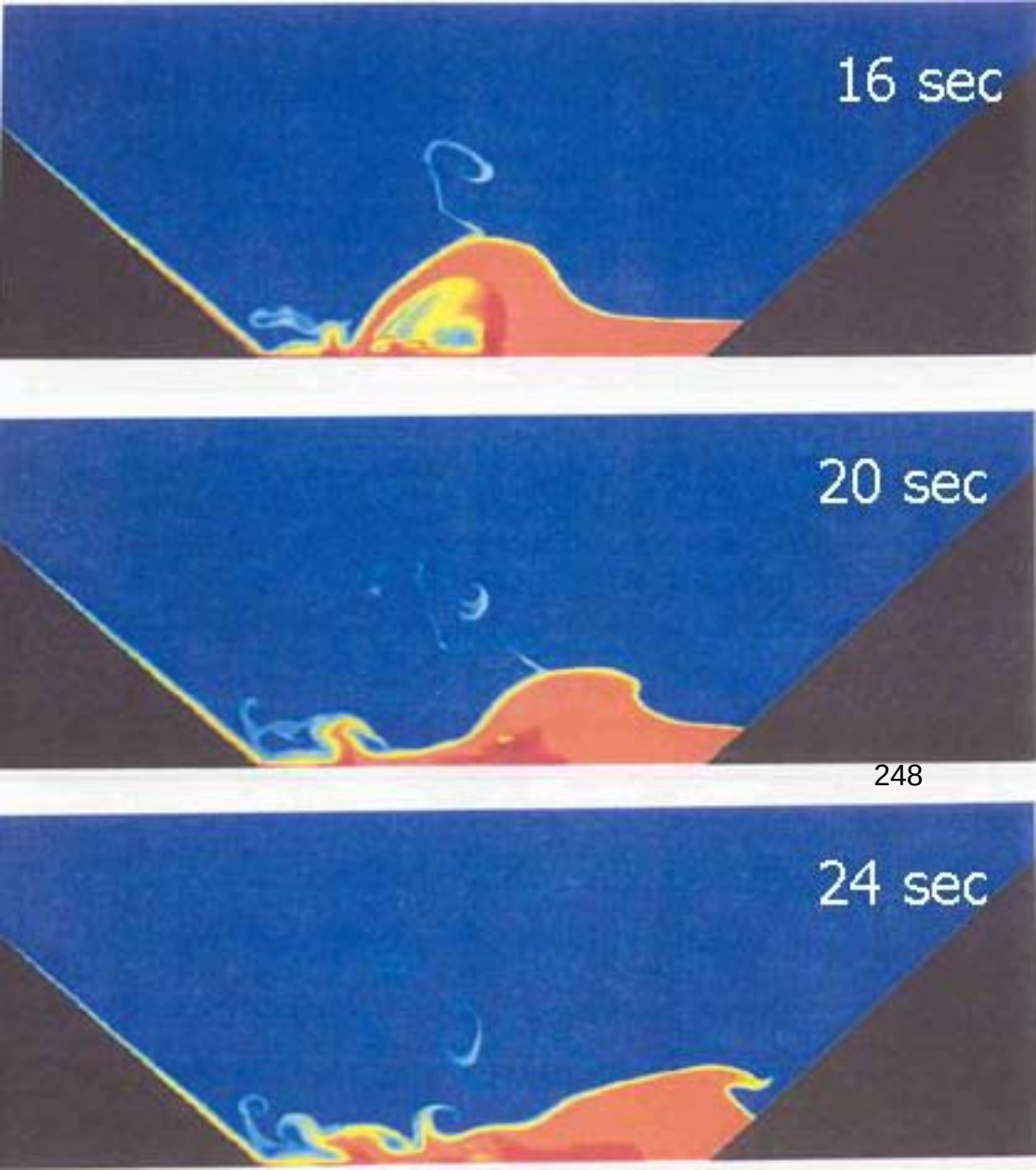
16 sec
20 sec
24 sec


26 sec


30 sec


34 sec

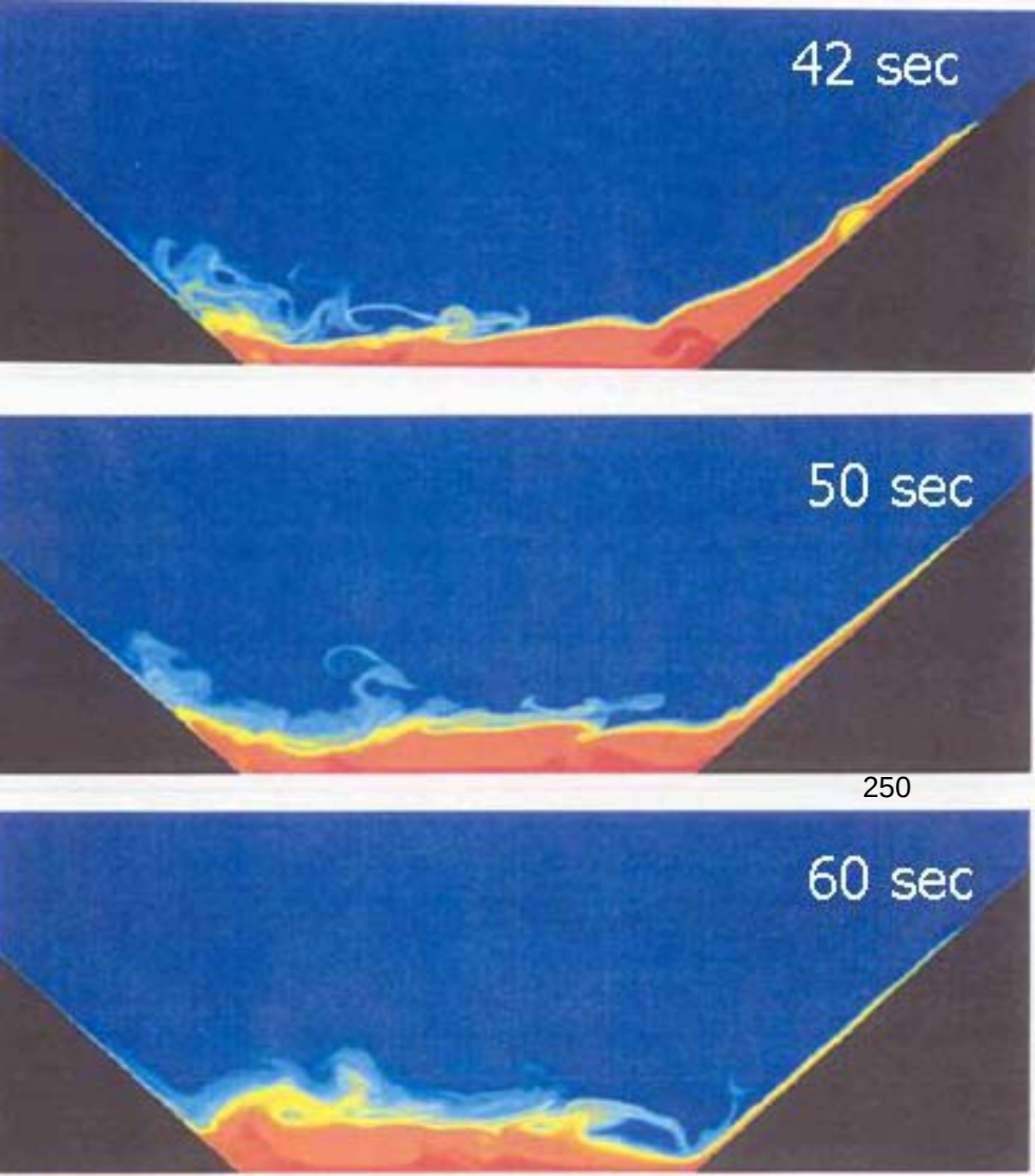
42 sec
50 sec
60 sec

EVALUATION OF THE THREAT OF MEGA TSUNAMI GENERATION FROM POSTULATED MASSIVE SLOPE FAILURES OF ISLAND STRATOVOLCANOES ON LA PALMA, CANARY ISLANDS, AND ON THE ISLAND OF HAWAII

George Pararas-Carayannis
Honolulu, Hawaii

ABSTRACT

Massive flank failures of island stratovolcanoes are extremely rare phenomena and none have occurred within recorded history. Recent numerical modeling studies, forecasting mega tsunami generation from postulated, massive slope failures of Cumbre Vieja in La Palma, Canary Islands, and Kilauea, in Hawaii, have been based on incorrect assumptions of volcanic island slope instability, source dimensions, speed of failure and tsunami coupling mechanisms. Incorrect input parameters and treatment of wave energy propagation and dispersion, have led to overestimates of tsunami far field effects. Inappropriate media attention and publicity to such probabilistic results have created unnecessary anxiety that mega tsunamis may be imminent and may devastate densely populated coastlines at locations distant from the source - in both the Atlantic and Pacific Oceans.

The present study examines the assumptions and input parameters used by probabilistic numerical models and evaluates the threat of mega tsunami generation from flank failures of island stratovolcanoes. Based on geologic evidence and historic events, it concludes that massive flank collapses of Cumbre Vieja or Kilauea volcanoes are extremely unlikely to occur in the near geologic future. The flanks of these island stratovolcanoes will continue to slip aseismically, as in the past. Sudden slope failures can be expected to occur along faults paralleling rift zones, but these will occur in phases, over a period of time, and not necessarily as single, sudden, large-scale, massive collapses. Most of the failures will occur in the upper flanks of the volcanoes, above and below sea level, rather than at the basal decollement region on the ocean floor. The sudden flank failures of the volcanoes of Mauna Loa and Kilauea in 1868 and 1975 and the resulting earthquakes generated only destructive local tsunamis with insignificant far field effects. Caldera collapses and large slope failures associated with volcanic explosions of Krakatau in 1883 and of Santorin in 1490 B.C., generated catastrophic local tsunamis, but no waves of significance at distant locations. Mega tsunami generation, even from the larger slope failures of island stratovolcanoes, is extremely unlikely to occur. Greater source dimensions and longer wave periods are required to generate tsunamis that can have significant, far field effects. The threat of mega tsunami generation from massive flank failures of island stratovolcanoes has been greatly overstated.

Science of Tsunami Hazards, Volume 20, Number 5, page 251 - 277 (2002)

INTRODUCTION

In recent years, there has been interest on the potential for mega tsunami generation from asteroid impact, large underwater slides and massive slope failures of oceanic island stratovolcanoes. Improved technology for sea floor mapping has helped identify features on the ocean floor that are indicative of large-scale kinematic processes in the distant geologic past. New satellite technology has helped identify slow processes of crustal subsidence and gradual slope failures of island volcanoes. Progress in the numerical simulation of tsunamis has been phenomenal. Supercomputers now provide realistic simulations of tsunami generation from asteroid impact and from explosions. Sophisticated software has allowed the modeling of all types of new tsunami generative mechanisms - leading to the development of better models of tsunami hazard assessment.

In spite of the advances, and in order to apply effectively the new computer technology for tsunami simulations, researchers must still make realistic assumptions of various generative mechanisms and use correct input functions in their models. Furthermore, in publicizing the results of probabilistic numerical modeling studies, there should be a clarification of what constitutes a near-term tsunami threat from that which may be caused from rare events, hundreds, thousands, or even hundreds of thousands of years from now. In order to plan and effectively mitigate the effects of the tsunami hazard, the assessment of risk must stay in the realm of what it is realistic now or in the near future (Pararas-Carayannis, 1988). Inappropriate media attention and misinterpretation of probabilistic research results for postulated rare events, can create unnecessary anxiety and negate present disaster mitigation efforts.

In view of extreme forecasts of mega tsunami generation and media publicity about the threat to coastal communities from the collapse of stratovolcanoes - the present study reviews the capabilities and limitations of numerical modeling, in general, in making accurate tsunami forecasts. More specifically examined are the input parameters and assumptions that were used in modeling tsunami generation from postulated massive flank collapses of the Cumbre Vieja volcano on the island of La Palma in the Canary Islands and of the volcano of Kilauea, on the island of Hawaii. Based on available geological data and a review of historical events, the present study further examines the likelihood that such massive volcanic flank failures can indeed occur in the foreseeable future, as postulated. Further evaluated are the reliability of the numerical models in simulating realistically the tsunami coupling mechanism and in forecasting accurately near and far field tsunami effects. The 1868 and 1975 earthquakes along Kilauea's southern flank are examined as to the type of slope failures that occurred and the resulting tsunami wave generation. Also, the caldera collapses and large slope failures associated with the volcanic eruptions of Krakatau in 1883 and of Santorin in 1490 B.C., are reviewed for the type of waves they generated and for the near and far field tsunami effects. Finally, conclusions are presented on whether the postulated flank failures at LaPalma and Kilauea can occur in the near future and whether these can generate mega tsunamis that pose a realistic threat to densely-populated coastlines, far from the source region.

POSTULATED COLLAPSES OF STRATOVOLCANOES AND PURPORTED THREAT OF MEGA TSUNAMI GENERATION

Stratovolcanoes in the Canary, Cape Verde, Hawaiian, Reunion, and other oceanic islands , show common constructional and structural features, such as rift zones, progressive slope instability and past flank gravitational collapses (Carracedo, 1999; Moore et al, 1989, 1994, 1995; Moore & Clague 1992; Moore & Chadwick, 1995). At least ten major flank collapses have occurred in the Canary Island chain in the past million years. Based on this, it was estimated that a major collapse can occur somewhere in the Canaries every 10,000 years or so (Day et al. 1999). The volcano of Cumbre Vieja on the island of La Palma was identified as unstable and as a likely site for a major collapse that would presumably generate a mega tsunami (Ward & Day, 2001).

Similarly, there is evidence that major landslides have occurred in the Hawaiian islands in the past. The Kilauea volcano on the island of Hawaii was identified as another site where a major flank collapse

would generate a mega tsunami (Ward, 2001). Although no specific time frame for these postulated collapses has been provided, it was inferred that they could be induced by the next volcanic eruption of Cumbre Vieja on La Palma, or by the next major earthquake near the Kilauea volcano in Hawaii.

Figure 1. La Palma and the other Canary islands

The postulated collapse of the Cumbre Vieja volcano on the island of La Palma: The volcanism that has formed LaPalma and the rest of the Canary islands, is the result of transition from continental (Africa) to oceanic (Atlantic) lithosphere. La Palma is an intraplate oceanic island built by composite volcanoes on the continental rise of the Northwest African Margin. It is the largest of the western Canary Islands, rising 6500 m. above the surrounding ocean floor (Fig 1). The Cumbre Vieja volcano on La Palma is a very active stratovolcano. Studies of the evolutionary structural development of Cumbre Vieja's rift zones (Day, et al, 1999), indicate changes in zone geometry, disparities in activity, underlying dyke swarms along the North-South trending main zone, and - following a 1949 eruption - the development of a normal fault system along the crest of the volcano. The geometry of this fault system and the timing of its formation, in relation to episodes of vent opening during the 1949 eruption, have led to the interpretation that this is not a surface expression of volcanic dike activity, but the result of a developing zone of weakness and of deformational instability. The observations resulted in concern that the volcano's steep western flank could undergo a large-scale, gravitational collapse which could occur suddenly with little or no precursory deformation.

The postulated collapse of the Kilauea volcano on the island of Hawaii: Measurements obtained by satellites of the Global Positioning System, documented that a 12 by 6-mile area (amounting to about 72-square-miles) of the south slope of Hawaii's Kilauea Volcano moved 3.5 inches toward the sea, over a 36-hour period in November 2000. The event, termed as a "silent earthquake," had energy equivalent to that of an earthquake with moment magnitude of 5.7. (Cervelli, et al., 2000)." This aseismic slip event has been interpreted as a possible prelude to the triggering of another sudden, massive slope failure of the underwater portion of Kilauea's southern flank.

Purported threat of mega tsunami generation: Based on the interpretation of geological and volcanological observations on the island of La Palma, a subsequent numerical tsunami modeling study was undertaken by Ward &. Day (2001), postulating that a massive landslide, with a volume of up 500 cubic km, could be triggered by the next major eruption of Cumbre Vieja. The study concludes that the collapse of Cumbre Vieja's western flank would generate a destructive mega tsunami which would strike both sides of the North and South Atlantic. Waves of up to 50 m. in height were estimated for Florida and the Caribbean islands, and more than 40 m. for the northern coast of Brazil. Although not as high, destructive waves have been forecast for the western coast of the Iberian Peninsula, France and Britain's Atlantic coastline. Presumably, in certain areas, the tsunami waves would travel as much as six to seven km. inland, destroying everything in their path.

The aseismic slip event on the southern coast of the island of Hawaii, was also interpreted as

possible prelude to the triggering of another sudden, massive slope failure of Kilauea's southern flank. Computer modeling of such postulated, massive flank failure (Ward, 2001) forecasts that a Pacific-wide, mega-tsunami would be generated. The study concludes that most of the energy of the mega tsunami will be directed toward the southeast, in the direction of Ecuador, but that coastlines as far away as California, Chile, and Australia will be also endangered. Waves as high as 30 m have been forecast for the west coast of North America, and up to 20 m. high for the southwest Pacific.

Unfortunately, media publicity of these estimates has inadvertently created unnecessary public anxiety, by further implying that the threat to coastal communities may be imminent, in both the Atlantic and the Pacific. The subsequent analysis demonstrates that these estimates are incorrect and that the threat of mega tsunami generation from the slope failures of stratovolcanoes has been greatly overstated.

EVALUATION OF NUMERICAL TSUNAMI MODELING METHODS - CAPABILITIES AND LIMITATIONS

Before evaluating the threat of mega tsunami generation from the postulated flank collapses of island stratovolcanoes, it is important first to review - in general - the capabilities and limitations of numerical modeling methods in making such predictions.

There is no doubt that, regardless of the nature of a tsunami's source mechanism, computer modeling has made the job of predicting near and far field wave effects particularly easier, especially when verification and calibration with historical tsunami data can be accomplished. However, problems still exist and errors and artifacts may be introduced which may affect significantly the modeling results (Kowalik, 2002). The accuracy of numerical models in estimating near and far field tsunami effects, depends on initial input parameters derived from realistic assumptions of generative mechanisms. For example, the simplest of the hydrodynamic models are usually based on linear dispersive wave theory which acceptably describes tsunami propagation and energy flux in the deep water. Input condition of the maximum elevation of water surface of the leading waves is correlated to source ground motion characteristics, as well as to the distance of the site from the source. What models like these cannot describe adequately, is the shallow water effects, which are due to the nonlinear nature of the tsunami. These are phenomena such as mach stem, bores, etc., in which nonlinear effects are essential. Also, considering the nonlinear aspects of tsunamis, numerical models have to consider accurately mesh, various grids for deep and shallow water, mesh refinements, irregular meshes, and the input functions which may be derived from the nonlinear models.

In determining tsunami propagation and runup heights, finite difference models have been used extensively with varying success. Comparison of the output of such models with analytical models, while necessary, does not always warrantee that the model is satisfactory. Most applications described in the scientific literature, allow for the moving boundary, the shoreline, to avoid the introduction of high spatial frequencies. Assumptions are usually made about spatial conditions existing in the neighborhood of a moving boundary resulting in the development of a flooding scheme which allows the governing differential equations to be applied without prejudice, uniformly across the computational grids.

Recently, great progress has been achieved in numerical tsunami simulations. For example, using supercomputers, researchers at the U. S. Los Alamos National Laboratory and Science Applications International Corporation, developed a compressible Eulerian hydrodynamic code which permits three-dimensional modeling of tsunami generation, propagation and inundation from a variety of tsunami source mechanisms - including asteroid impact (Weaver et al, 2002). These new models provide for very realistic graphic representations - in the form of three-dimensional moving simulations - showing the result of finite differences at every time step. Viewing of such graphics allows evaluation of the model performance, the detection of computational anomalies, the adaptation of mesh refinement techniques, and the assessment of spatial and temporal coherency. Also, these new methods allow for various formulations of the nonlinear advection term to be tested for stability and to examine the effects by filtering.

In summary, therefore - and to be realistic - all numerical studies of tsunami source coupling wave

propagation and terminal effects must make valid assumptions on the correlation of the initial water displacements to tsunami wave length and period in the source region, regardless of the generative mechanism - whether an earthquake, a landslide, or an impact event such as a rockfall or an asteroid. Various source models and scenarios of generation/impact must be examined. Terminal characteristics of the tsunami and flooding can only be approximated by linear calculation for a given shore which is close to the source. However, such terminal tsunami characteristics, require nonlinear treatment when dealing with distant sources. Verifications of the models is essential through the use of analytical solutions with experimental results. If possible, such verification should be accomplished with historical data - as presently being done for the National Tsunami Hazards Mitigation Program -. or even with a pneumatic landslide generator, as it was done for the 1958 Lituya Bay tsunami (Mader 2001; Mader & Fritz, 2002).

Unfortunately no model verification can be obtained for mechanisms of massive lateral collapses of volcanic island stratovolcanoes, as none - having the postulated source parameters - have occurred within recorded history. Although extremely useful, ultimately the accuracy of all numerical models in determining near and far field tsunami effects - regardless of apparent sophistication - is based on assumptions of initial input parameters related to the tsunami source mechanism. And this is where the problem lies with modeling tsunamis from postulated slope failures of island stratovolcanoes. As demonstrated in the following sections, improper assumptions of source parameters and unrealistic coupling mechanisms, can often result in erroneous input parameters in modeling tsunami generation. Mistreatment of dispersion and of nonlinear shallow water effects, can further result in unrealistic estimates of both near and far-field tsunami terminal effects.

ANALYSIS OF ASSUMPTIONS AND INPUT PARAMETERS USED IN MODELING MEGA TSUNAMI GENERATION FROM POSTULATED COLLAPSES OF THE OCEANIC ISLAND STRATOVOLCANOES OF CUMBRE VIEJA ON LA PALMA, CANARY ISLANDS, AND OF KILAUEA, IN HAWAII

As previously stated, sudden and massive flank failures are extremely rare phenomena. There is evidence that the flanks of island stratovolcanoes fail, but there is no scientific consensus on why or how this happens. Furthermore, there is no valid geologic evidence documenting that prehistoric collapses generated mega tsunamis with significant far-field effects. The recent numerical studies (Ward & Day, 2001; Ward 2001) forecasting mega tsunami generation from recurrences of large massive volcanic island flank failures, are based on unrealistic assumptions of present slope instability of Cumbre Vieja on La Palma and Kilauea in Hawaii, of source dimensions, of speed of failure, and of tsunami coupling mechanisms. Incorrect treatment of input parameters and of wave energy propagation and dispersion, produced incorrect estimates of near and far field terminal effects - thus overstating the tsunami threat.

In order to evaluate the threat of mega tsunami generation from the postulated massive flank failures, we much review the assumptions and input functions used by the recent modeling studies. First, we will examine if massive volcanic collapses are possible at the present time and if they can occur, as postulated. Subsequently, we will review if the models developed correctly the necessary input functions, and if proper coupling mechanisms were used to arrive at the source dimensions and initial modeling parameters. Then, we will examine if realistic input conditions were properly applied in calculating wave travel, energy distribution, geographical spreading and dispersive effects, and in forecasting near and far field tsunami heights. Finally, in assessing the validity of the above numerical models, we would need verification with historical events. Historical tsunami runup data can help assess on whether effects of spatial and temporal coherency were taken into consideration by these models, and generally evaluate model performance and prediction capability - for both near and far field effects. Unfortunately, this cannot be done as massive flank failures of volcanic island stratovolcanoes are extremely rare events. Purported deposits of paleo-tsunami runup activity on the islands of Lanai, Molokai and elsewhere (McMurtrya et al. 1999), are of questionable validity. Therefore, comparisons will be made with some recent historical events, for which there is data.

Present volcanic flank instabilities and past collapses: The recent numerical studies (Ward & Day, 2001, Ward 2001) - forecasting mega tsunami generation - are based on incorrect assumption that the underwater flanks of the Cumbre Vieja and Kilauea volcanoes are extremely unstable and that massive failures can occur in the near future.

Indeed, in the distant geologic past, massive slides occurred in the Canary, Cape Verde and Hawaiian islands as well as elsewhere in the Atlantic, Pacific and Indian oceans. Prehistoric, massive landslides and flank failures of oceanic island stratovolcanoes have been extensively studied and documented in the scientific literature (Moore et al, 1989, 1994, 1995; Moore & Clague 1992; Lipman, 1995; Moore & Chadwick, 1995; Clague et al., 1998; Carracedo et al. 1999; Dartnell & Gardner, 1999; Day et al. 1999; Day et al. 1999b; Mehl & Schmincke, 1999; Moss et al., 1999; Rileya et al 1999; Smith et al. 1999; Stillman, 1999). However, the mechanisms of prehistoric volcanic flank failures are not fully understood and are still under scientific investigation.

More frequently, stratovolcanoes appear to slide fairly easily along the bases - often aseismically. Generally the movement is continuous. However, occasional locking has been responsible for some rather large slope failures and destructive earthquakes. When the failures occur suddenly, they are not particularly massive. Although local destructive tsunamis are often generated, within historic times, volcanic flank failures have not generated destructive waves for shorelines distant from the source region.

As with all oceanic island stratovolcanoes, the underwater flanks of Cumbre Vieja and Kilauea are composed mostly of layers of pillow lavas, interspersed with smaller volumes of pyroclastics. Ordinarily, these materials are relatively stable and not susceptible to massive, monolithic failures. Presently, there is no sufficient geological evidence to support that La Palma's west flank or Hawaii's southern flank are critically unstable or that a massive failure can be expected. However, partial flank failures, as in 1868 and 1975 in Hawaii, may be expected every two hundred years or even more frequently (Pararas-Carayannis, 1976a, 1976b).

Flank instability of La Palma: The evolution of the western Canary islands, especially in their earlier stages of growth, has included giant lateral flank collapses (Carracedo, et al 1999). La Palma, together with El Hierro and Tenerife, are the youngest of the western Canary Islands and still in their active shield volcanic stage, which began almost 7.5 Ma ago (Stillman, 1999), with zones which were subsequently underlain by swarms of dikes and other minor intrusions (Walker, 1999). La Palma has rugged topography with peaks rising to several thousand meters. A brief review of La Palma's geology indicates that it was formed by three stratovolcanoes. The northern part of the island was formed by the shield volcano Taburiente, about two million years ago (Figure 2). The giant Caldera de Taburiente, is a large depression 5 km across, with an area of 30 sq. km, and 2 km deep, increased to this size by extensive erosion and landslides. The central and southern part of La Palma were formed by the two other volcanoes, Cumbre Nueva and Cumbre Vieja. Giant landslides and erosion during the past million years have removed more than half of the total sub aerial volume of La Palma. At least one catastrophic collapse, the Cumbre Nueva giant landslide, occurred about 560 ka ago. The collapse removed some 200 km3 of the central-western part of La Palma, forming a large embayment. (Carracedo, et al., 1999).

Recent eruptive activity on La Palma occurs on Cumbre Vieja, which has a concentrated volcanic center aligned primarily along a well-defined, N-S trending rift zone - in which major dike emplacement has taken place (Stillman, 1999). The structural reconfiguration of Cumbre Vieja's rift zones - which begun about 20 ka ago - the development and high activity of the dominant south trending rift, the underlying dike swarms, and surface changes which followed the 1949 eruption, have led to the conclusion that the volcano's western flank is presently at an incipient stage of flank instability (Day et al,.1999).

Indeed, Cumbre Vieja's western flank appears to be relatively unstable. However, and in spite of its apparent instability, it highly unlikely that a major flank collapse will occur in the near future - particularly one that could be greater than the prehistoric Cumbre Nueva landslide, of about 560 ka ago. Further review of La Palma's geologic structure indicates that the island is composed of two main rock layers separated at about 427 m above sea level. The lower layer is made of pillow lavas, cut by basaltic

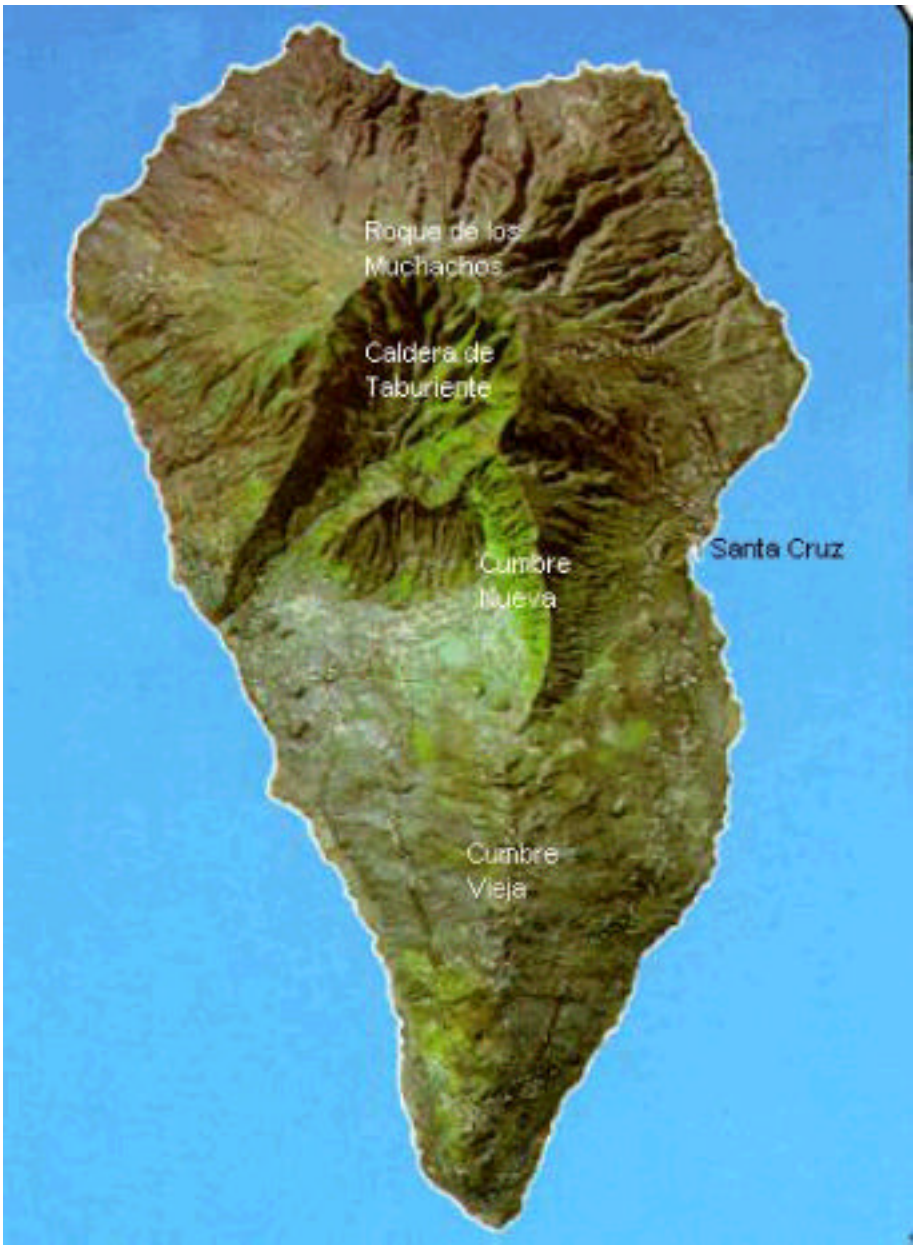

Figure 2. Relief Map of the island of La Palma showing the volcanoes of Taburiente, Cumbre Nueva Cumbre Vieja and the north-south trending rift zone and secondary faults.

dikes. The thickness of the pillow lavas ranges from 10 to 350 m. The upper layer consists of basaltic lavas and pyroclastic rocks. In certain areas, as in the Caldera de Taburiente, strong erosion over time has resulted in the accumulations of large volumes of gravels, mixed with basaltic lava flows. Similar erosion, but to a lesser extent, has taken place also along Cumbre Vieja's flanks. Therefore, a massive surface failure on Cumbre Vieja's flank is very unlikely to occur. The existing basaltic flows and dikes, the latter located within 3 km on the west coast of the island and extending underwater, would limit significantly the volume of material of any slope failure, above or below the water. Surface flank failures on La Palma would have limited dimensions and would occur, either in a step-like form or

contained by ring dikes - as those observed along the flanks of the Piton de LaFournaise volcano on Reunion island in the Indian Ocean (Fig 3). As for a massive failure of the western flank along a deeper detachment surface, there is still not sufficient or conclusive geologic evidence that it can happen in the near future - as postulated by the tsunami modeling studies.

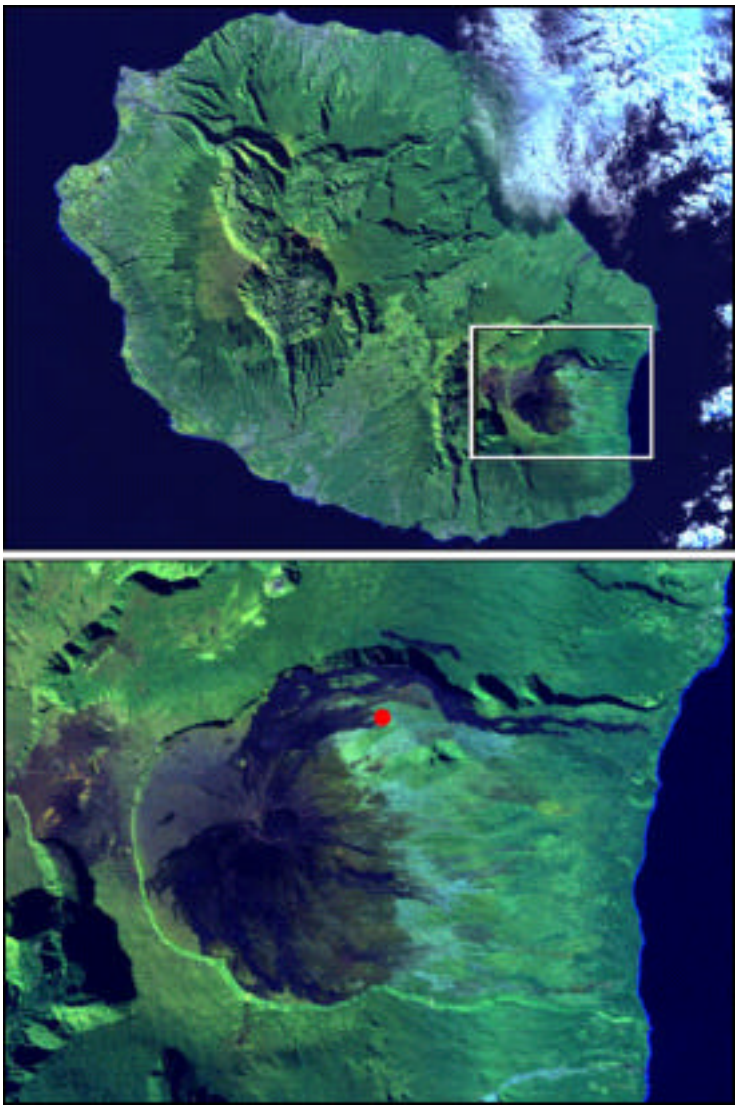

Fig. 3. Reunion Island in the Indian Ocean and the Piton De La Fournaise volcano showing extensive erosion, subsidence and an arcuate coastline suggestive of underwater slope failure.(Source: GEOSAT photos)

Flank instability of Hawaii: Review of the submarine geology of the island of Hawaii, shows evidence of debris avalanches on the ocean floor along the southwestern flank of the Mauna Loa volcano. The debris avalanches - composed of large blocks, pulverized rock, and water - are indicative of large prehistoric slides. (Moore et al. 1989, 1994; Lipman, 1995; Moore and Chadwick, 1995; Clague et al., 1998; Dartnell and Gardner,1999). Above water, the slope of Mauna Loa is unusually steep. There are no large escarpments or faults to indicate gradual slippage in recent times (Lipman, 1995) . However, gradual subsidence has occurred in the past along the southern flank. The magnitude 8.0 Kau

earthquake of 1868, resulted in extensive subsidence of the southern flank of Mauna Loa, which also affected the southern flank of Kilauea.

Review of the coastal geology along Kilauea's southern flank, indicates a different pattern of kinematic processes. A number of coastal fault scarps, some as high as 500 m., parallel the Puna rift zone and are the tops of an extensive fault zone known as the Hilina Fault System, along which substantial movement has occurred in the past (Fig. 4). Large fault blocks are tilted back, by as much as 8° towards the rift zone, indicating a pattern of gradual subsidence. This subsidence has created the feature known as Hilina Slump. Papa`u Seamount is the submarine expression of the active Hilina Slump (Morgan et al 2001) (Fig. 5).

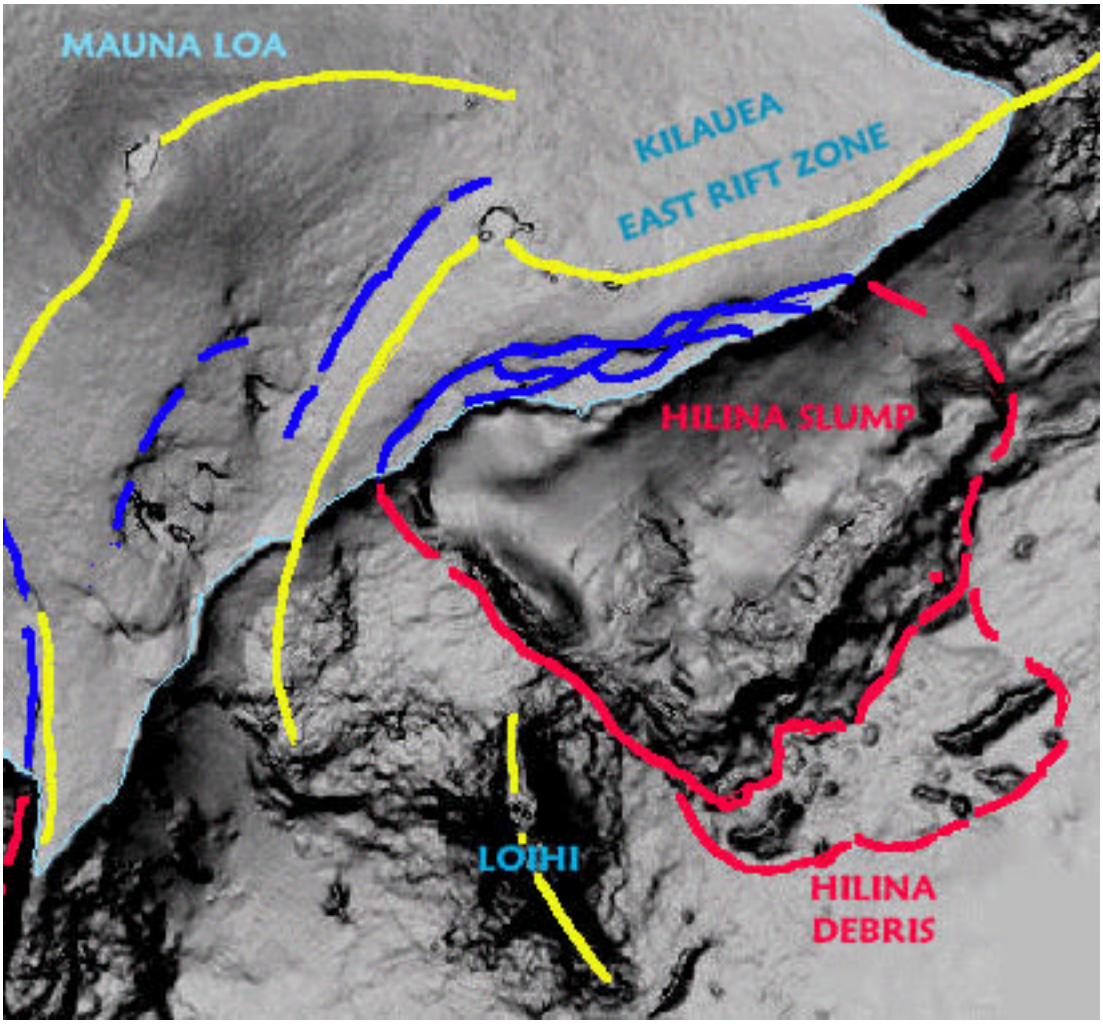

Figure 4. Hawaii's southern slope showing coastal faults parallel to the east rift zone of the Kilauea volcano, and the Hilina Slump along which slope failures have been occurring (Modified after Morgan et al. 2001).

Paleomagnetic studies of changes in lava flow directions on the Hilina Fault scarps have helped determine the pattern and speed of subsidence along the southern flank of Kilauea. In addition to subsidence, these studies have determined a pattern of counterclockwise rotation, indicating slippage between blocks, occurring along listric normal faults (Rileya et al., 1999)

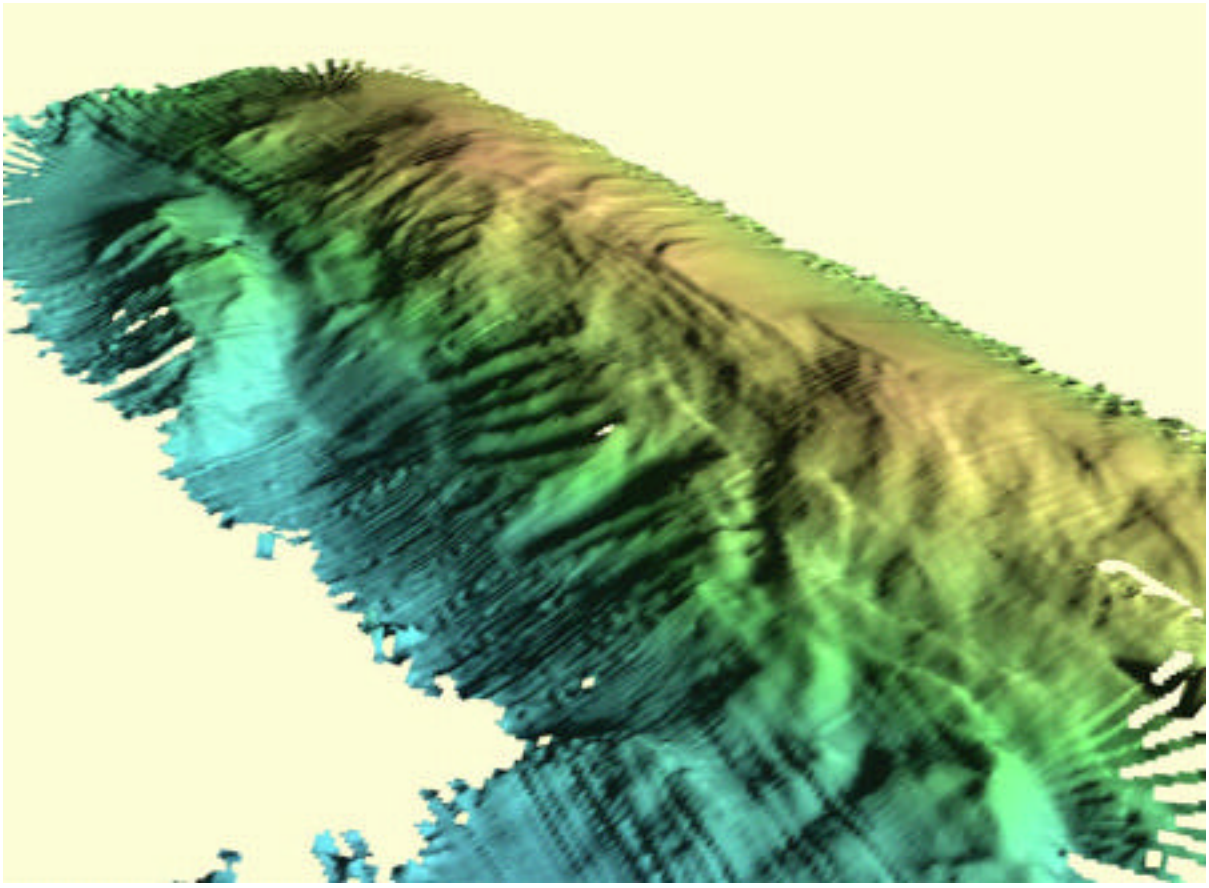

Fig. 5. Oblique sidescan view of the Papa`u Seamount (Modified after(Smith et al, 1999)

During the 1990's, Kilauea appeared to be sliding easily along its base, in a seaward direction, at an average speed of about 10 cm a year. The aseismic slip event - which was detected in November 2000 by GPS measurements along this southern slope - occurred gradually over a 36-hour period. Although indicative of some degree of instability, the motions were imperceptible and occurred along the upper slope of Kilauea's southern flank (Cervelli et al, 2000). Such slow aseismic movements have probably occurred over thousands of years. These imperceptible kinematic changes are now being detected and measured, only because new satellite technology and instrumentation have made it possible.

In summary, there is no indication that Kilauea's southern flank is unusually unstable at this time, or that a catastrophic massive, failure can occur as postulated by the recent tsunami modeling studies (Ward 2001). The subsidence process on the Hilina Slump appears to be continuous and gradual. High-resolution side scan surveys of Kilauea's southern slope (Clague et al 1998; Dartnell and Gardner 1999) show a number of cuspate normal faults near the head of the slump, as well as grabens and horsts. These are indicative of past successive, crustal movements - some associated with major earthquakes. As documented in a subsequent section, not even the large earthquakes of 1868 and 1975 were associated with large-scale slope failures along Hawaii's southern coast. Neither of these two significant earthquakes generated a destructive Pacific-wide, mega tsunami (Pararas-Carayannis 1976a, 1976b, Pararas-Carayannis and Calebaugh, 1977). However, it should be pointed out that a repeat of the 1975 flank failure and associated large earthquake, can be expected on the south flank of Kilauea every 200 years or even more frequently (Pararas-Carayannis, 1976a, 1976b).

.

EVALUATION OF MASSIVE VOLCANIC FLANK FAILURES ALONG DETACHMENT FAULTS

The recent numerical studies (Ward & Day, 2001, Ward 2001) - forecasting mega tsunami generation - are based on incorrect assumption that the flanks of the Cumbre Vieja and Kilauea volcanoes are extremely unstable and that massive failures along detachment surfaces can be expected in the near future.

As stated, recent research indicates that stratovolcanoes can move or slide along their bases. The movements are relatively continuous and result in gradual subsidence and slumps. Much of this movement appears to take place at the volcano/sea floor boundary or along parallel zones of weakness inside the volcano. These zones of weakness are often referred to as detachment faults, along which limited subsidence often occurs. Occasional locking and subsequent sudden slippage along these internal zones of weakness, or near the sea floor base, can cause sudden movements and large earthquakes. Both La Palma and Hawaii appear to have such zones of weakness and, as shown, massive flank failures occurred in the distant past. However, no catastrophic flank collapses along detachment faults have occurred within recorded history. Recent flank failures in Hawaii have been limited in extent. Although Cumbre Vieja, on La Palma, appears to be sliding in a seaward direction at the present time, the volcano is stable during inter-eruptive periods. There is no indication that a massive collapse along a detachment surface will occur when the volcano again erupts.

Evaluation of postulated massive flank collapse along a detachment fault zone on La Palma: The tsunami modeling study (Ward & Day, 2001) is based on a massive flank collapse initiating along a detachment fault on La Palma . An extensive rupture - with maximum offset of 4 meters - along Cumbre Vieja's crest is the purported surface expression of a major discontinuity along which the collapse will occur (Figure 3).

As with Kilauea, the Cumbre Vieja volcano appears to be sliding in a seaward direction. However, contrary to Kilauea - where palis of up to 500 m in height can be found - there no extensive fault system paralleling Cumbre Vieja's major N-S trending rift zone. Furthermore, there is no seismic or geologic data to support that the 4 m near-summit rupture on Cumbre Vieja is indeed the purported zone of weakness along the western flank - or that it extends to the volcano's base, as postulated. Indeed the summit rupture resulted in west-facing normal faulting during the 1949 eruption (Day et al.,1999). Its geometry and the timing of its formation in relation to episodes of vent opening during the eruption suggests the possible development of a discontinuity beneath the volcano's western flank, along which a collapse or substantial slope failure may occur in the distant future. However, the apparent seaward displacement measurements by a ground deformational network and by the Global Positioning System are within the error-margins of the techniques employed (Moss et al. 1999). Although the apparent movement vectors do suggest a coherent westward displacement to the west of the 1949 fault system, the results are not conclusive as to the instability of Cumbre Vieja's western flank, or that a collapse is imminent.

There is nothing to support that any massive type of failure will soon occur along this detachment boundary - if indeed it extends to the volcano's base - as postulated. Further review of La Palma's geology shows that all of the recent historical volcanic eruptions on La Palma were associated with about 120 volcanic vents which are distributed along the crest of Cumbre Vieja's rift zone. In view of this distribution and the absence of seismic data, it is also conceivable that the near-crest rupture that developed in 1949, is only a shallow geomorphological feature, rather than the surface expression of a deeper discontinuity surface. It may have been caused by superficial gravitational settling, such as that which forms double step calderas, or from partial collapses of magmatic chambers that supplied lava to the numerous vents, along the volcano's north-south trending rift zone. Furthermore, even if this rupture is indeed a surface expression of an extensive, deeper discontinuity, there is still no basis that a flank collapse can occur along this zone of weakness as a single, massive event. A maximum offset of only 4 meters cannot be evidence of substantial failure or extreme instability. In spite of magmatic intrusions from Taburiente's magmatic chamber to the north, and other than the Cumbre Nueva giant landslide, of

560 ka ago, none of the known major historical eruptions of Cumbre Vieja, the latest in 1971, triggered any significant flank or slope failures (Fig. 6). There is no sufficient data to support that a major collapse of Cumbre Vieja will occur along the postulated discontinuity, when the volcano again erupts.

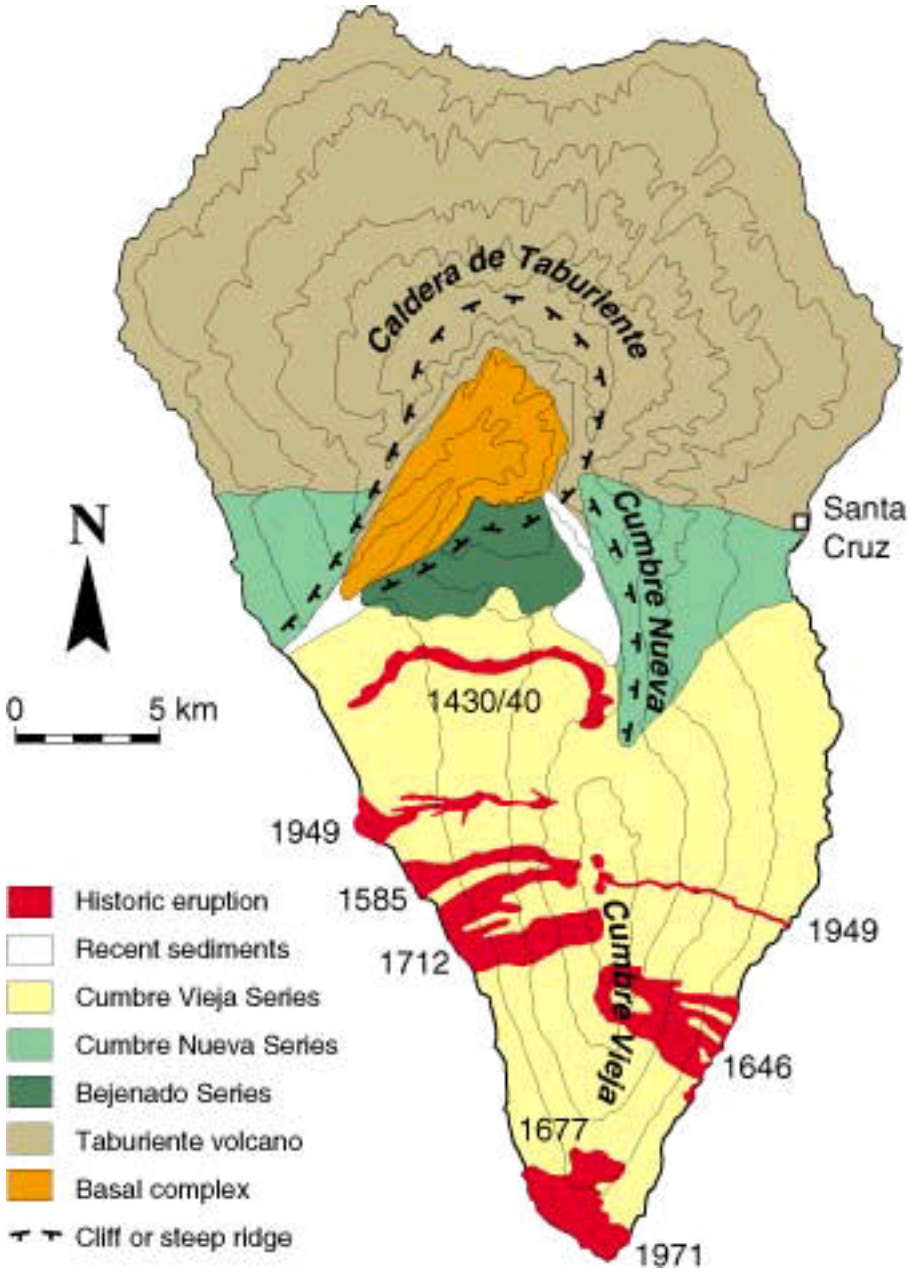

Figure 6. Geological map of La Palma island showing sites of historic eruptions of the Cumbre Vieja volcano from vents along its north-south trending rift zone.

Evaluation of the postulated massive flank collapse along a detachment fault zone on Hawaii: Tsunami modeling by Ward (2001) is based on the premise of a massive flank failure along a

detachment surface along Kilauea's southern flank in Hawaii. In contrast to La Palma, in Hawaii there is geologic evidence of an extensive zone of flank weakness, primarily along the southern flank of Kilauea. Paralleling the Puna rift zone, there is an extensive system of coastal faults (palis) which appear to be gravitational features associated with ongoing subsidence caused by both seismic and aseismic events - the latter also documented by recent GPS satellite measurements. There is also evidence of other parallel submarine volcanic rift zones, formed in an evolutionary sequence (Reynolds et al. 1998). Marine geophysical data, including SEA BEAM bathymetry, HAWAII MR1 sidescan, and seismic reflection profiles, indicate that the southern slope of Hawaii comprises the three active hot spot volcanoes Mauna Loa, Kilauea, and Loihi seamount and is the locus of the Hawaiian hot spot (Smith et al, 1999). As stated, the Hilina Slump is the offshore continuation of the mobile Kilauea volcano south flank and has resulted from subsidence and slope failure along a deeper detachment surface. The sub-aerial portion of the slump creeps seaward at a rate of approximately 10 cm/year. The south flank is characterized mostly by frequent, low-intensity seismicity. Most of the sudden crustal movements which have generated strong shallow earthquakes in the past, appear to be triggered by intrusions and lava movements in the magmatic chambers below the volcano. However, in spite of the apparent instability, a massive flank failure of Kilauea along a detachment fault zone - as postulated (Ward 2001) - is very unlikely to occur. Neither the 1868 nor the 1975 earthquakes were associated with massive flank failures of Mauna Loa or Kilauea or generated an ocean-wide mega tsunami (Pararas-Carayannis 1976a, 1976b, Pararas-Carayannis and Calebaugh, 1977).

EVALUATION OF TRIGGERING MECHANISMS OF VOLCANIC FLANK FAILURES AND COLLAPSES

Tsunami modeling (Ward & Day, 2001; Ward, 2001) is based on assumptions that a major volcanic eruption on La Palma, or a major earthquake in Hawaii, will trigger massive flank collapses on these islands. There is no mention of what lateral or vertical forces are needed to initiate the failures. Also, inferred by the modeling studies are: a) that the triggering forces act on the center of an unstable flank mass - otherwise there could not be a monolithic movement; and b) that the unstable flank mass has monolithic coherence - even though composed of pillow lavas and loose pyroclastics.

Slope instabilities, slope failures and gravitational flank collapses of island stratovolcanoes can be caused by different mechanisms, individually or in combination. Triggering mechanisms may include isostatic load adjustments, extensive erosion, gaseous pressures, violent phreatomagmatic eruptions, magmastatic pressures, gravitational collapse of magmatic chambers, dike and cryptodome intrusions as well as buildup of hydrothermal and supra hydrostatic pore fluid pressures.

Basic physics of slope failure: Assuming that a massive, monolithic slope failure of an island can indeed occur along a deeper "detachment surface", we must still look for the forces that are needed to trigger it. Review of slope failure mechanism can only be based on the following considerations (Fig. 7). If only gravity is the acting force, there are two components. One component is acting perpendicularly to the slope of this detachment surface, the other is acting tangentially. The perpendicular component of gravity (gp) holds the potential slide material (pyroclastics, pillow lavas) in place. The tangential component of gravity (gt) causes a shear stress parallel to the slope - which tends to pull an unstable block in the downslope direction.

If the slope (along which failure can occur) increases, the tangential component of gravity on that potential mass of slide (gt) increases, and the perpendicular component of gravity (gp) decreases. The forces resisting downward movement would be shear strength, which includes frictional resistance and cohesion among the particles that make up the mass of the potential slide. When the shear stress becomes greater than the combination of forces holding the mass of the slide on the slope or along a detachment surface, then the slide or a collapse are triggered. The failure will occur more readily on steeper slope angles which increase the shear stress. Any other external influence that would tend to reduce shear strength - such as lowering the cohesion among the particles of the mass or lowering the

frictional resistance - could be a triggering mechanism for the failure.

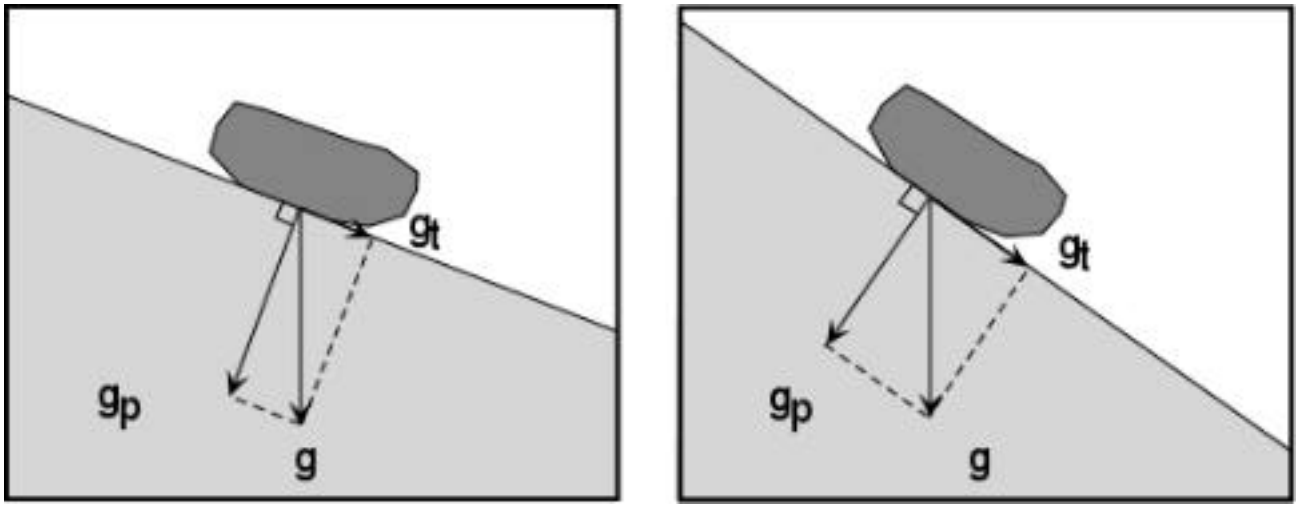

Fig. 7. Physics of Slope Instability

The modeling studies of a La Palma collapse (Ward & Day, 2001) do not comment on forces needed to overcome the shear strength and mass inertia of a postulated 500 cubic km block of material, or at which point of this unstable mass the forces must act to trigger its movement and subsequent collapse. Since the models treat the initial flank failure as monolithic, as stated previously, the inference is that the force of an event - whether a volcanic eruption or an earthquake - triggers it by acting near the center of the mass. However this is an unrealistic assumption because for movement or a collapse to occur, slope failure must initiate closer to the base of the mass, or at least near the center of mass (if monolithic) rather than at its upper portion.

Magmatic chamber collapse mechanism: Gravitational collapse of unsupported magmatic chambers can exert shear forces primarily in the direction parallel to the postulated failure, rather at the more effective right angle. However massive caldera collapses are usually associated with violent Strombolian, Surtsean, Plinian and Ultra-Plinian volcanic eruptions rather than with eruptions of shield volcanoes. The triggering mechanism of the last violent paroxysmal eruptive phase of a colossal or super-collosal volcanic eruption such as those of Krakatau and Santorin, may be hydromagmatic or the result of extreme gaseous pressures building below high viscosity magmatic residues. Usually, caldera collapse occurs by the engulfment of the unsupported upper cone into the drained magmatic chambers of a volcano after the final paroxysmal phase. However, in the case of the Krakatau or Santorin, the estimated volumes of ejected pumice and other pyroclastic debris were considerably less than the volumes of the caldera depressions (Pararas-Carayannis, 2002). The volume discrepancy suggests a possible mechanism for the explosive removal of the upper volcanic cone, rather than its total engulfment, or perhaps a combination of the two processes. Also, the volume discrepancy may be related to the size of empty magmatic chambers, to lateral material movement, and to adjacent underwater slope failures. Caldera collapse is not necessarily a sudden and total process. Often, the collapse process occurs in phases. This may result in the formation of ring dikes indicating post-collapse magmatic intrusion along fractures formed by the subsidence of the roof of the magma chamber.

Regardless of the form or severity of volcanic explosive activity, collapse processes on any volcano may create large depressions that resemble Krakatoan calderas, or double pit craters such as those observed at the summit of shield volcanoes like Kilauea in Hawaii, or Taburiente on LaPalma. Erosional processes and slides, as with the extinct Taburiente or Koolau volcanoes, can contribute significantly to the post-eruption enlargement of calderas.

There is no evidence of significant magmatic chamber collapse along the crest of Cumbre Vieja, as the apparent reservoir of magma appears to be under the Taburiente volcano to the north. So this does not appear to be a potential mechanism for large scale flank failure on La Palma. On Kilauea's summit, there is a large caldera which is indicative of magmatic chamber collapse. However the present caldera appears to be quite stable. Limited crater collapses have occurred along Kilauea's rift zone, but again this is not considered to be an effective mechanism for triggering any massive type of collapse.

Isostatic mechanism: Although the main force responsible for any slope failure is always gravity, an event of considerable force is needed to trigger the movement of a large mass, as postulated. Slope failure due to gravity alone, is a function of the angle of repose at which the volcanic materials were deposited as the islands built up. On the flat ocean floor surface, the force of gravity acts downward, so nothing moves. On a young volcanic island - still in its shield building phase - extruded lava flows find their own natural angles of repose, above and below the water. Excluding the influence of other forces, underwater slopes of young volcanoes are relatively stable, consisting mainly of pillow lavas. As a stratovolcanic island builds up and loads the earth's crust, isostatic adjustments cause flank subsidence, buckling of the ocean floor, and offshore deeps and arches. For example, the morphology and structural evolutionary development of the Hilina Slump, off Kilauea's southern coast, suggest an active isostatic adjustment process. The Hawaiian Trough and the Hawaiian Arch are examples of isostatically-caused buckling of the ocean floor around the island of Hawaii. Although accountable for the continuous mobility of the volcanic flank, as observed along the southern coast of Hawaii, this mechanism is too slow to trigger sudden collapses.

Erosional mechanism: As a volcanic island gets older, extensive erosion takes place. The deposited materials consist primarily of unconsolidated sediments, gravels, rocks, pyroclastics, or lavas flows reaching the sea from subsequent flank or summit eruptions. Where a large accumulation of loose material occurs, the flank becomes less stable. Gravity alone, or the vertical and horizontal accelerations of an earthquake, can trigger landslides.

Erosion during the Miocene period played a key role in the evolution of Fuerteventura and Lanzarote, the oldest of the easternmost Canary Islands. Giant landslides reduced them considerably in height (Stillman, 1999). Even on La Palma, El Hierro and Tenerife, the younger western islands, which are still in their shield stage, substantial amount of erosion has occurred. On La Palma, hundreds of meters of sedimentary material - primarily gravel - has accumulated on the western slope of the island primarily due to extensive erosion of the Taburiente caldera. The gravel is mixed with basaltic lave flows, a trend which appears to continue into the ocean. A large surface landslide could be triggered by a large earthquake. However the existing volcanic dikes would render some stability. Overall the erosion mechanism can be effective in triggering landslides, particularly on the older islands, but not on flanks of volcanoes, still in their shield building stage. Therefore, it is very unlikely that a massive surface landslide of great dimensions can occur by this mechanism on either La Palma or Hawaii. In Hawaii, for example, the major earthquake of 1868 only triggered a surface landslide on Mauna Loa that was only three miles long and thirty feet thick.

Gaseous pressure mechanism: To overcome the shear strength of 500 cubic km of material on LaPalma, as postulated, would require a very large triggering event and a tremendous lateral shear stress. Gaseous pressures do not built up on shield type of volcanoes as they do prior to the paroxysmal Plinian and Ultra-Plinian eruptions of the Krakatoan variety. Most of the eruptions of Cumbre Vieja and Kilauea are non-explosive types and involve primarily extrusions of pahoehoe and aa lavas, with only small amounts of pyroclastics, usually from secondary vents.

In the case of La Palma, a major volcanic eruption of Cumbre Vieja, either near the summit or along vents of its rift zone, would not build up great gaseous pressures and could not exert sufficient shear stress to trigger failure at the base of the postulated mass - most of which is underwater. Recent eruptive activity on Cumbre Vieja occurs along a concentrated volcanic center aligned primarily with a well-

defined North-South trending rift zone in which major dike emplacement has taken place (Stillman, 1999). Deformation by intruding magma can indeed create a local stress field which may result in predominantly dip-slip motion and form a rupture - as the one resulting from the 1949 eruption. However, such triggering mechanism will affect the upper portion of the volcano and can only result in partial flank failure.

Phreatomagmatic mechanism: Phreatomagmatic eruption activity due to ground water intrusion - from increased rainfall activity, caused by climatic changes - has been proposed as another possible triggering mechanism for volcanic flank failures and giant landslides (McMurtrya et al. 1999). As the magmatic system comes into contact with the hydrothermal system, the expansion of water - in the form of superheated steam - results in an explosive type of activity that tends to weaken a volcano, perhaps to the point of collapse. This would be particularly true for continental type of volcanoes that involve Strombolian, Vulcanian, Peléean or Plinian type of eruptions, but not so much on oceanic shield volcanoes. At the latter, phreatomagmatic activity is usually limited to secondary cone eruptions and the emissions of tephra or ephritic lava. Furthermore, on oceanic island volcanoes, this mechanism tends to initiate primarily sub aerial collapses which may be usually limited to the upper flanks or along secondary vents along the rift, which may be nearer to the coast.

Additionally, and regardless of climate changes and wetter periods, relatively young volcanic islands such as Cumbre Vieja and Kilauea - still in the shield building stage - retain little ground water because of greater rock porosity. Most of the rain water runs off and is lost. There is no extensive water lens at the base, as with older and highly eroded volcanic islands. On the younger volcanic islands rainfall water collects in pools, surrounded by impermeable dikes - usually in the upper slopes. Any violent phreatomagmatic activity is usually limited to a few vents near the summit or the upper flanks of the volcano and involves only shallow magmatic chambers. In fact, in 1949, there was a 5-week-long magmatic and phreatomagmatic eruption activity along Cumbre Vieja's ridge (White & Schmincke, 1999). There was no evidence of large scale collapse.

The 1949 eruption begun with emission of ephritic lava from five vents at the Duraznero crater on the ridge top of Cumbre Vieja (1880 m above sea level). After these vents shut down abruptly, activity shifted to an off-rift fissure at the Llano del Banco crater, located at 550 m lower elevation and 3 km to the northwest. The new eruptive center emitted initially tephritic aa but later emissions were basanitic pahoehoe lava (Klügela et al, 1999). Two days after the initial basanite emissions began at Llano del Banco, the Hoyo Negro crater (at 1880 m above sea level), located 700 m north of the Duraznero crater along the rift, begun producing ash and bombs of basanitic to phonotephritic composition, in violent phreatomagmatic explosions (White and Schmincke, 1999). However, the covariance in the eruption rates of vents that was observed during Llano del Banco's and Hoyo Negro's simultaneous phreatomagmatic activity, is indicative of a rather shallow hydraulic connection and of a limited ground water supply. Other than a few modifications within the southwestern margins of Hogo Negro's crater - 50 to 100 m lower (White & Schmincke, 1999), the phreatomagmatic components of the 1949 eruption did not cause any large failure of Cumbre Vieja's flank. Similarly, there have been no large-scale hydromagmatic eruptions on Kilauea and no landslides of any significance have been generated. In view of these observations, it can be concluded that phreatomagmatic activity is limited on active stratovolcanoes and will not cause massive flank collapses.

Forced dike injection mechanism: The forced injection of dikes and the concurrent development of mechanical and thermal pore fluid pressures along the upper flank or at the basal décollement region, combined with associated magmastatic pressures at the dike interface - as proposed by Elsworth & Day (1999) - can indeed contribute to significant destabilization of the flank of an active stratovolcano, such as Cumbre Vieja or Kilauea. Whether a shallow flank or a deeper basal décollement failure will eventually be triggered, will depend on additional complementary destabilizing effects of mechanical magma "piston like push" at the rear of the weakened block, and the buildup of thermal and supra hydrostatic pore pressures - if below the water table. Depending on the geometry and horizontal extent of dike intrusion and its thickness, as well as on the extent of contributing hydrothermal and mechanical

factors, such combined forces can indeed become an effective primary triggering mechanism for larger-scale volcanic flank failures and subsequent tsunami generation.

There is evidence that large, prehistoric flank failures were triggered by such mechanisms. Dike and cryptodome intrusion, as well as hydrothermal alteration in the crater area, probably weakened and further triggered the flank collapse of the Roque Nublo stratovolcano on Gran Canaria Island during the Pliocene period (Mehl & Schmincke, 1999). The massive, prehistoric, collapse of the Monte Amarelo volcano on Fogo, in the Cape Verde island group, appears to have been induced by radial rift zones fed by laterally propagating dikes (Day et al 1999b). More recent eruption on Fogo, in 1951 and 1995, appear to be associated with episodes of flank instability caused by now vertically propagating dikes which manifested in normal faulting near the volcano's rift zone.

Proper interpretation of seismic data is crucial in making reasonable predictions of volcanic flank instability associated with forced dike injection, before or during a major eruption. For example, seismic data was used successfully to distinguish between brittle fracture of cold host rock and deformation in the vicinity of intruding magma for the 1995 Fogo eruption in the Cape Verde Islands (Heleno da Silva et al., 1999). Based on composite seismic focal mechanism analysis, the size, depth and direction of the dike feeding the eruption were identified. From this, an estimate of the associated stress field was obtained and correlated with the volcano's flank topography.

Lateral magma migration appears to have occurred on La Palma, beginning in 1936. Stronger seismic harmonic tremors begun in early March 1949. Their foci distribution suggests that magma ascended from chambers beneath the Taburiente volcano and moved along the north-south-trending rift of Cumbre Vieja (Klügela et al, 1999). As already mentioned, a major eruption, with phreatomagmatic activity, begun at Duraznero crater on the ridge top (1880 m above sea level) on June 24, 1949. The occurrence of xenoliths almost exclusively near the end of the eruption is indicative of wall-rock gravitational collapse at depth. The eruption was associated with subsidence and left a two kilometer-long fracture near the summit.

The volcanic evolution of the 1949 eruption of Cumbre Vieja seems to be typical for La Palma. Prior to and during each eruption, there appears to be considerable shallow magma migration, which is manifested by strong seismicity, intense faulting, and the opening of closely spaced vents (Klügela et al, 1999). However, it should be noted that none of the historic eruptions in 1430/40, 1585, 1646, 1677, 1712, 1949 or in 1971, triggered a large size slope collapse. on the island. Although the flank of Cumbre Vieja may have been somewhat destabilized by the 1949 and 1971 eruptions, there is no indication that a critical condition has been reached, or that the next major eruption will trigger a massive flank failure.

In all cases, forced injection of dikes and kryptodomes - and the concurrent development of mechanical and thermal pore fluid pressures - appear to result in seaward movement of the volcanic flank and may eventually result in partial failures of larger scales. It is believed that mechanical magma intrusion, primarily, and buildup of thermal and supra hydrostatic pore pressure, secondarily , are the more effective mechanisms for the sudden and larger scale volcanic flank failures that can generate local destructive tsunamis. Such was the apparent mechanism for major past flank failures of Mauna Loa and Kilauea volcanoes along the southern coast of Hawaii, and the cause of the 1868 and 1975 earthquakes - neither of which generate a destructive Pacific-wide mega tsunami (Pararas-Carayannis, 1976a, 1976b, 2002). Finally, it should be noted that even the colossal and super-collosal, Plinian and Ultra-Plinian eruptions of Krakatoa and Santorin volcanoes in 1883 and 1490 B.C. - which were associated with massive flank failures - generated a mega tsunami that was destructive far away from the source regions (Pararas-Carayannis, 2002).

EVALUATION OF SOURCE DIMENSIONS OF POSTULATED FLANK COLLAPSES

The recent tsunami modeling studies (Ward & Day, 2001, Ward 2001) used unrealistic source dimensions of flank collapses that are even greater than those of prehistoric events. The postulated Cumbre Vieja collapse is based on a massive monolithic slide block 15-20 km wide, 15-25 km long and

up to 500 cubic Km in volume. Similarly unrealistic are the source dimensions for the postulated flank collapse of Kilauea along Hawaii's southern coast.

Indeed, there is abundance of geologic evidence indicating that several large-scale flank collapses have occurred in the distant past, in the Canary, the Cape Verde, the Hawaiian and other volcanic islands. The prehistoric flank collapse of the Monte Amarelo volcano on Fogo island in the Cape Verde archipelago, had an estimated volume of at least 150-200 km3 (Day et al 1999b). The Pliocene, flank collapse of the Roque Nublo volcano on Gran Canaria island left debris deposits of at least 14 km3, covering an area of about 180 km2, in the southern half of the island (Mehl & Schmincke, 1999). There was at least one known catastrophic collapse on La Palma about 560 ka ago. This was the Cumbre Nueva giant landslide, which removed an estimated 200 km3 of the central-western of the island, forming a large embayment. (Carracedo, et al 1999).

The Hilina slump is the only large submarine landslide in the Hawaiian Archipelago thought to be still active. Over millions of years, the slump is estimated to have covered an area of 2100 km2 and a displacement having a volume of 10,000-12,000 km3 (Smith et al. 1999). However, its geomorphology indicates that slope failures occurred from numerous discrete small events, over a period of time. Also, superimposed on the Hilina slump are horsts and grabens - indicative of gravitational subsidence and of lateral pressure effects from dike and cryptodome intrusion originating from shallow magmatic chambers of Kilauea and Mauna Loa volcanoes. As discussed in the next section, all of the known historical earthquakes on the southern part of the island of Hawaii involved relatively limited slope failures and generated only destructive local tsunamis in 1823, 1868 and in 1975 (Pararas-Carayannis, 1967, 1976a,b). In 1989, this same region again experienced smaller, damaging earthquakes, but with limited subsidence and no significant tsunami generation. Although the overall dimensions of the Hilina slump are great, the distinct historical episodes of slope failures had limited dimensions.

The April 2, 1868 slope failure of Mauna Loa: The most destructive tsunami of the 19th Century was generated by a local earthquake (Pararas-Carayannis, 1967, 1975) with an estimated magnitude of 7.75 (Furumoto, 1966). The shock was felt throughout the Hawaiian islands, as far as Niihau some 350 miles away. On the island of Hawaii, strong ground motions triggered a landslide, which was three miles long and thirty feet thick. The slide swept down a hill killing thirty-one people and thousands of cattle, sheep, horses, and goats. Later, on April 28, lava broke out on the southwest flank of the Mauna Loa volcano and created a 15-mile flow to the sea.

The 1868 earthquake was associated with considerable subsidence along the flank of the Mauna Loa volcano. According to Brigham (1868), the most destructive tsunami effects were observed over a distance of 50 miles along Hawaii's southern coast. Brigham could not determine whether the "shoreline has been raised or depressed" but all indications are that it was depressed, since the water first recessed before waves inundated the coast. Tsunami waves struck the coast from Hilo to South Cape, being most destructive at Keauhou, Puna, and Honuapo; 180 houses were washed away, and 62 people lost their lives. A 10-foot-high wave carried wreckage inland 800 feet. At Honuapo all houses were destroyed. A stone church and other buildings were destroyed at Punaluu. The place presently known as the Keahou Landing on the southern part of Hawaii is what Bingham refers in his description as Keahou. Maximum tsunami wave height there was 65 feet, the highest observed in Hawaii to date (Pararas-Carayannis, 1967, 1975).

The November 29, 1975 slope failure of Kilauea: The major earthquake of November 29, 1975 (surface wave magnitude of 7.2), somewhat to the east of the area affected by the 1868 event, involved uplift, subsidence and slope failure. It generated another destructive local tsunami. Maximum horizontal crustal displacement was approximately 7.9 meters. Near Keauhou Landing, maximum vertical subsidence was approximately 3.5 meters. The displacements decreased to the east and west from this area. In fact, subsidence rapidly decreased to the west. At Punalu'u, the shoreline actually uplifted by about 10 centimeters (Pararas-Carayannis 1975). Subsequent surveys determined a subsidence of about 3 meters at Halape Park to the east. A large coconut grove area adjacent to the beach subsided by as much as 3.0 and 3.5 meters. Further to the east, the subsidence decreased to 1.1 meters at

Kamoamoa, 0.8 meters at Kaimu, 0.4 meters at Pohoiki, and 0.25 meters at Kapoho. According to the Volcano Observatory of the U.S. Geological Survey, even the summit of Kilauea subsided by about 1.2 meters and moved towards the ocean by about the same amount. A small, short-lived eruption took place inside Kilauea's caldera.

The affected offshore block was approximately 70 km long, and 30 km wide with the long axis of the displaced block being parallel to the coast. This entire offshore region rose approximately 1.2 meters. The total volume of displaced material was roughly estimated to be only 2.52 cubic km (Pararas-Carayannis 1976a,b). Furthermore, inspection of tide gauge records showed the initial wave motion to be upwards at all stations. The significance of this observation is that the offshore crustal displacement was an uplift, as the onshore section subsided and moved outward. This was indicative that the resulting slope failure and earthquake were not entirely due to gravitational effects of instability, but may have been partially caused by compressional lateral magma migration from shallow magmatic chambers of Kilauea. or by lateral magmastatic forces along an arcuate failure surface or along a secondary zone of crustal weakness on the upper slope of the Hilina slump. In fact, recent paleomagnetic studies show that differential rates of movement and rotation occur between sections of the slump (Rileya et al., 1999).

Finally, it is interesting to further note that Hilo was greatly affected by the earthquake shock waves in 1868 and in 1975, but not by the tsunami waves. This is suggestive of the directionality of slumping and of the limited dimensions of distinct slope failure events along the southern flanks of Kilauea and Mauna Loa. Neither of these two slope failures generated a mega tsunami that posed a threat at locations distant from the source. Slope failures and subsidences along Kilauea southern flank have occurred with frequency. However, the failures appear to have occurred in phases, over a period of time, and not necessarily as single, large-scale events, involving great volumes of material.

Slope failures from the volcanic explosions of Krakatau in 1883 and Santorin in 1490 B.C. : The violent colossal and super-collosal, Plinian and Ultra-Plinian, volcanic explosions of Krakatau in 1883 and of Santorin in 1490 B.C. resulted in large caldera and flank collapses. Combined with atmospheric shock waves, they generated the most destructive local tsunamis of volcanic origin, in recorded history. Although the source dimensions and volume of material involved were great, it should be noted that the flank failures were significant but not particularly massive.

The explosion/collapse of Krakatoa generated formidable tsunami waves that were up to 37 m in height. However, the tsunami was only destructive locally in Indonesia. Only small waves were recorded away from the source region (Pararas-Carayannis 2002). Similarly, the great explosion/collapse and flank failures of Santorin generated a very destructive tsunami estimated to be 40-50 m high near the source area. However, at Jaffa-Tel Aviv, 900 km away, the maximum height of the tsunami had attenuated to about 7 m tsunami (corrected for eustatic change) (Pararas-Carayannis, 1973, 1992).

EVALUATION OF SLIDE SPEED

Tsunami modeling of the La Palma collapse (Ward & Day (2001) is based on the conjecture that a massive failure of a large crustal block - up to 500 cubic Km in volume - cascades 60 km out to sea in only 10 minutes, by rafting on a highly pressurized layer of mud or fault gouge breccia, before reaching rest at the flat portion of the ocean, at 4,000 meters. A similarly high slide speed is used to model tsunami generation from a massive collapse along Kilauea's Hilina Slump region, in Hawaii (Ward, 2001). The models treat the slides as monolithic rotations along "detachment faults", rather than turbulent movements of large size materials, such as pyroclastics and pillow lavas. The effects of water turbulence behind the slides' masses, are ignored. It is further assumed that the slides move, monolithically, for the first 15 km, at a specified constant velocity of more than 250 km/hour (about 70 - 100 m/s).

The models ignore cohesion among the particles of the mass that would tend to resist movement. The postulated slide speeds of 70-100 m/sec - which have appeared also elsewhere in the the scientific literature - are based on conjecture. They are unrealistic as they would already be the speed of a tsunami

in 50 m of water depth. Furthermore, the speed of a tsunami in 50 m is the speed of potential energy propagating on the surface of the ocean, while the speed attributed to the slides is that of kinetic energy along the bottom.

Since the postulated collapses are presumably rotational along detachment faults, there is also an implicit assumption that the slope of the failing surface is reduced with depth. However, the modeling studies do not take into proper consideration the effect that slope reduction would have on the slide's speed. Reduction of slope would slow down the slide rather than accelerate it to 100 m/sec. Large boulders of pillow lavas cannot possibly move that rapidly. Frictional effects which would tend to slow down the slide's speed, are overlooked by assuming lubrication from instantaneously-formed fault gouge breccia.

The speed of flank failure used by the models, is simply unrealistic. The maximum speed of the 1929 Grand Banks slide was less than 80 km/h. which is less than the postulated slide speeds used for La Palma and Hawaii slides. Furthermore, the Grand Banks slide involved unconsolidated sediments which could move rapidly downslope as turbidity currents with much less friction (Piper et al 1988). The mostly, large size particles of pyroclastics and the pillow lavas of Cumbre Vieja or Kilauea, cannot move as fast as turbidity currents. Finally, rapid crustal movements, usually of the upper portion of a stratovolcano's flank, could only occur along fault fractures triggering an earthquake, dike intrusion, or a magmatic chamber collapse - either as a linear features or along a ring dike. Such mechanisms would tend to limit the extent, dimensions and speeds of a potential slide. Failures would result either from compressional effects or from gravitational adjustments. The time history of such failures would be fairly short in duration. Frictional effects - which would tend to put the breaks on slides - are disregarded by the numerical models. Ultimately, the efficiency with which waves can be generated will depend on how close the slide speed is to the tsunami speed in that depth of water.

EVALUATION OF LANDSLIDE COUPLING MECHANISM AND INITIAL TSUNAMI AMPLITUDE

The numerical models (Ward & Day, 2001, Ward 2001) further assume that the initial tsunami amplitude can be estimated on the basis of being proportional to the vertical center of a slide's mass displacement (Murty, 1979; Watts 1998, 2000). However this would be a reasonable approximation only if the slope failure was a monolithic event, and the mass moved as a unit downslope without disintegrating in the process - and without taking into consideration the effects of water turbulence behind the slide or the effects of bottom friction. However, this is not how slope failures actually occur in nature. Furthermore, and as mentioned previously, moving 500 cubic Km of material, as postulated for LaPalma, would require a tremendous triggering force acting on the center of gravity of a block, and the slide would need to start from a resting position.

As a result of incorrect assumptions on source dimensions, slope instabilities and slide speeds, the numerical tsunami models (Ward & Day, 2001, Ward 2001), overestimate the initial parameters of slide-to-water coupling. The problem is further exacerbated by the manner of the numerical computation. For example, in developing the model's depth grids, depth averaging is used - which is an acceptable method when used to simplify tsunami generation by an earthquake. However, this cannot work for landslide failure mechanism because of differences in time scales. As a slide moves downslope, water flows around it in the opposite direction. But depth averaging assumes that slide and water move together, which leads to an incorrect coupling mechanism in these models.

EVALUATION OF TSUNAMI FAR-FIELD EFFECTS FROM POSTULATED COLLAPSES OF STRATOVOLCANOES

The combined effects of erroneous assumptions on source dimensions, source ground motions, speeds and coupling mechanisms of the La Palma and Kilauea collapse models (Ward & Day, 2001,

Ward 2001) produce initial leading tsunami waves that are far too high. By treating the resulting tsunami as a shallow water wave, the models treat incorrectly wave height attenuation with distance away from the source. The models further overlook the following basic principles.

Regardless of generative mechanism, there is always scattering and dispersion of energy over a wider geographical area as tsunami waves propagate away from a source region. Changes are due to refraction primarily (large refractive indices tend to produce correspondingly large dispersions), but geometrical spreading will also affect tsunami wave heights and, ultimately, runup at a distant shore. Source dimensions, geometry of the tsunami generating area and coupling mechanisms, determine the initial heights and periods of the resulting waves and whether these will propagate as shallow or intermediate waves. If the wavelengths are short, dispersion will have a greater effect in attenuating heights away from the source region. In general, dispersion increases toward shorter wavelengths, and varies approximately inversely with the cube of the wavelength.

Also, because of the earth's sphericity, geometric spreading reduces the wave energy - and wave height - with distance traveled. The tsunami energy will begin converging again at a distance of 90 degrees from the source. Geometrical spreading will have a greater effect for long period tsunami waves. For example, for two dimensional (X, Z) dispersive tsunami waves, the maximum height decay with distance is theoretically proportional to $x^{-1/2}$ at great distances from the source. For three-dimensional (r, S) dispersive tsunami waves, the height-change relationships with distance conforms to r^{-1}. The width of such three dimensional tsunami waves, propagating away from their generating source, at any time will be:

$$S = S_o \ sin \ \theta$$

Where So = widest wave front at an arcual distance of 90 degrees away from the source and (θ) is the great circle distance expressed in degrees.

For a constant depth ocean, the tsunami amplitude A is related to:

$$A^2 \propto S^{1/2} = \frac{1}{\sqrt{S_o \ sin \ \theta}}$$

$$or \quad A \propto (sin \ \theta)^{-1/2}$$

where S is the width of the tsunami wave front.

Even though the ocean does not have a constant depth, a first order approximation of offshore tsunami height with distance can be obtained, assuming a direct path and only spreading. Also, the lesser the width of the tsunami wave front and greater the distance away from the source, the greater will be the wave height attenuation. Recent modeling studies of tsunami generation from asteroid impact confirm that the height-change relationships with distance conforms to r^{-1}, in accordance to linear dispersive wave theory (Weaver et al., 2002).

The La Palma and Kilauea collapse models (Ward & Day, 2001, Ward 2001) treat the resulting

tsunami as a shallow water wave and also produce initial leading tsunami waves that are far too high. As a result, far field tsunami effects are greatly overestimated. For example, within two minutes after the postulated La Palma failure begins (15-25 km wide; mass 500 cubic km.), the model estimates a water dome 900 meters high on top of the monolithic slide block. After five minutes, and after traveling 50 km, on top of the now disintegrating block of material, the leading wave height drops to 500 meters**.** After ten minutes of travel - when the slide has reaches its rest on the ocean floor - the leading wave has grown to 250 km in diameter. By this time, purported mega tsunami waves of several hundred meters in height have already struck the other Canary islands. The leading wave of 200 meters propagating away from the source region, is followed by positive and negative waves that are now 2-3 times greater - 400 to 600 meters in amplitude. According to the model, mega tsunami waves of up to 50 m. in height reach Florida and the Caribbean islands and more than 40 m. the northern coast of Brazil (See Fig. 2). The modeling of the Kilauea collapse (Ward 2001), forecasts mega tsunami heights of up to 30 m for the west coast of North America, and up to 20 m for the southwest Pacific.

The far field forecasts of these models are erroneous for the following additional reasons. Even with the overstated source dimensions, the postulated collapse mechanism can generate only an initial wave of short wavelength. Maximum period cannot be more than 3-4 minutes. The wave will behave as an intermediate rather than a shallow water wave (Mader, 2001). By treating the resulting tsunami as a shallow water wave, the models only describe the geometric spreading and not the significant dispersion that shorter period waves undergo with distance away from the source. Thus, the models treat incorrectly wave height attenuation. The wave height is treated as being proportional to the square root of wave energy. Presumably, as the wave height increases during the postulated monolithic failure and coupling mechanism, the mass of water involved in the wave and its height above normal sea level, increases. Water turbulence behind the mass of the slide - which would tend to decrease both the energy and the wave height - is ignored. Essentially such modeling presumes that, somehow, waves generated from the postulated slides of LaPalma or Kilauea will increase in energy as they propagate away from their sources - in other words more energy will be generated than initially imparted. This is simply not possible.

Another implicit, erroneous assumption is that the wave energy decreases linearly with distance (in an ocean of constant water depth), and therefore dispersion will decrease the wave height with the square root of distance from source - thus much more slowly than predicted by linear dispersive wave theory. Furthermore, that this effect of dispersion will only decrease the wave height by 2/3rd or 3/4th of the root of distance from the source - further assuming incorrectly that the dominant wavelength increases - so that the eventual impact of the tsunami wave as it comes ashore is not so greatly reduced.

Thus, these models forecast incorrectly tsunami far field effects. Shallow water effects, which are due to the nonlinear nature of the tsunami, are treated as linear and overestimated. Only waves of much longer wavelength can propagate effectively across ocean basins. Even though local destructive tsunami waves can result from the postulated mechanisms, waves of such short periods will rapidly decay away from the source region with considerable height attenuation.

Subsequent modeling by Mader (2001) confirms this and provides realistic estimates of tsunami far-field effects for the same hypothetical La Palma slide. Using the wave profile output obtained from a high speed (110 meters/second), pneumatic landslide generator of the Swiss Federal Institute of Technology at Zurich, Switzerland (Fritz, 2001), and based on a "worst case" scenario for La Palma (650 meter high, 20 kilometer radius water wave after 30 kilometers of travel), Mader's numerical model treats the resulting tsunami as an intermediate wave of short wavelength and period - taking into account both dispersion and geometric spreading effects. Specifically, the shorter period and wave amplitudes in his model, result in significant wave height attenuation with distance - to less than one-third of the shallow water amplitudes. The upper limit of his modeling study shows that the east coast of the U.S. and the Caribbean would receive waves less than 3 meters high. The European and African coasts would have waves less than 10 meters high. However, full Navier-Stokes modeling of the same La Palma failure, brings the maximum expected tsunami wave amplitude off the U.S. east coast to about one meter.

SUMMARY AND CONCLUSIONS - ASSESSMENT OF THE MEGA TSUNAMI THREAT FROM POSTULATED COLLAPSES OF ISLAND STRATOVOLCANOES

Sudden, catastrophic, flank collapses of island stratovolcanoes are extremely rare phenomena and none have occurred within recorded history. Numerical modeling of mega tsunami generation (Ward &. Day, 2001, Ward 2001) has been based on unrealistic scenarios of massive flank collapses of volcanoes in La Palma, Canary islands, and the island of Hawaii. Indeed, stratovolcanoes appear to move or slide along their bases. However, most of their flank movements are relatively continuous and result in gradual subsidence and slumps - often aseismically. Much of the movements appear to take place at the volcano/sea floor boundary or along zones of weakness, paralleling volcanic rift zones. Occasional locking and subsequent sudden slippage along internal zones of weakness or near the sea floor base can cause sudden movements and large earthquakes. However, volcanic slope failures occur in phases, over a long period of time, and not necessarily as single, sudden, large-scale events. Most of the sudden failures in historic times have been limited in extent and did not involve great volumes of material. They have been shallow phenomena, usually occurring in the upper flanks, rather than at the basal decollement region. Overall, subsidences and slides appear to be triggered by gravitational settling,, by partial collapses of empty volcanic magmatic chambers, by isostatic adjustment processes, by magmastatic pressures at the dike interface but, principally, by the forced injection of dikes and kryptodomes and the concurrent development of mechanical and thermal pore fluid pressures along the upper flanks or at the basal décollement region of stratovolcanoes.

Review of geology and of historic events of LaPalma, does not support claims that the island's western flank is particularly unstable or that the next large volcanic eruption of the Cumbre Vieja volcano will trigger a massive failure along a detachment fault. There is no seismic data to support that an observed rupture along the crest of the volcano is the surface expression of a major weakness zone along which detachment and major failure can occur in the near future. A summit or flank eruption cannot exert sufficient shear strength to trigger the movement of up to 500 cubic km of material - as postulated. None of the eruptions of Cumbre Vieja on La Palma in 1646, 1712, 1949 or 1971 triggered a large size slope collapse or generated a mega tsunami. The 1929 Grand Banks landslide, which involved 300-700 cubic km of material, generated only a local tsunami with insignificant far-field effects. The 1958 rockfall that caused the 524 m. impact tsunami inside Lituya Bay was hardly noticeable outside the source region. The gigantic Plinian and Ultra-Plinian volcanic eruptions of Krakatau in 1883 and of Santorin in 1490 B.C. involved large scale slope failures and generated catastrophic local mega-tsunamis, but the waves rapidly decayed as they traveled from the source. The maximum wave recorded in Batavia (presently known as Jakarta), from the Krakatau explosion/collapse was only 2.4 meters. The waves at Jaffa-Tel Aviv in the eastern Mediterranean from the explosion/collapse of Santorin were only 7 meters high.

A similar review of the geology and of historic events of the island of Hawaii, does not indicate that Kilauea's southern flank is unusually unstable or that a massive collapse is possible in the foreseeable future. None of the strong earthquakes in Hilo in 1834, in Mauna Loa in 1938, or along the Kona coast in 1951, triggered an underwater slope failure or generated a tsunami. Neither of the 1868 or the 1975 major earthquakes on the southern coast of Hawaii resulted in major flank collapses. The slope failures were large but not massive. Other than local destructive tsunamis, these two events did not generate destructive waves at great distances away from the source region. The 1975 tsunami did cause limited damage to boats on Catalina island, near the California coast, but no waves of significance occurred there or anywhere else.

It is extremely unlikely that massive collapses on the islands of La Palma, or Hawaii will occur in the foreseeable future, as postulated. The modeling studies forecasting mega tsunami generation (Ward &. Day, 2001; Ward 2001) are based on erroneous assumptions of volcanic island slope instabilities, source dimensions, speed of failure, and tsunami coupling mechanisms. Incorrect input functions led to inaccurate output estimates as to near and far field tsunami effects. Even if the collapses occur as postulated, they can only generate waves of short wavelengths and periods that will be only locally destructive. These waves can only behave as intermediate rather than as shallow water waves. Thus, the

models treat incorrectly wave dispersion with distance and have overestimated greatly the far field effects. Dispersion will be significantly greater for waves of shorter periods and wavelengths that can be generated from the postulated mechanisms - even with the overstated source dimensions. The waves will rapidly decay and will not be a major threat away from the source regions.

A collapse of Cumbre Vieja will not generate waves of up to 50 m. in height in Florida and the Caribbean islands, or more than 40 m along the northern coast of Brazil, . Mega tsunami generation from the postulated collapse of Kilauea is equally unrealistic. Waves of up to 30 m for the west coast of North America, and up to 20 m for the southwest Pacific are not possible. Proper modeling of dispersive effects (Mader 2001) - provides much more realistic far-field wave estimates, in the unlikely event of a large-scale, La Palma slope failure. Mader's model of a La Palma slide estimates that the east coast of the U.S. and the Caribbean would receive tsunami waves of less than 3 meters and the European and African coasts would receive waves less than 10 meters high. However, this represents the upper limit. Full Navier-Stokes modeling brings the maximum expected tsunami wave amplitude off the U.S. east coast to about one meter. Even with shoaling effects, a tsunami from a La Palma slide would still be of concern but does not present an unmanageable threat or a significant far field hazard.

The threat of mega tsunami generation from collapses of oceanic island stratovolcanoes has been greatly overstated. No mega tsunamis can be expected - even if the lateral collapses of Cumbre Vieja in LaPalma and Kilauea, in Hawaii island occur, as postulated. Greater source dimensions and longer wave periods are required to generate tsunami waves that can have significant, far field effects.

REFERENCES

Carracedo , J. C. , 1999. *Growth, structure, instability and collapse of Canarian volcanoes and comparisons with Hawaiian volcanoes.* Journal of Volcanology and Geothermal Research, Vol. 94 (1-4) (1999) pp. 1-19.

Carracedo, J. C., Day S. J. , Guillouc H. and Pérez Torradod F. J., 1999. *Giant Quaternary landslides in the evolution of La Palma and El Hierro, Canary Islands.* Journal of Volcanology and Geothermal Research, Vol. 94 (1-4) (1999) pp. 169-190.

Cervelli, et al., 2000. *Sudden aseismic fault slip on the South Flank of Kilauea volcano.* (at web site).

Clague, D. A., Reynolds, J. R., Maher, N., Hatcher, G., Danforth, W., and Gardner, J. V., 1998. *High-Resolution Simrad EM300 Multibeam Surveys Near the Hawaiian Islands: Canyons, Reefs, and Landslides.* EOS, Transactions American Geophysical Union, 79, F826.

Dartnell, P. and J.V. Gardner (1999). *Sea-Floor Images and Data from Multibeam Surveys in San Francisco Bay, Southern California, Hawaii, the Gulf of Mexico, and Lake Tahoe, California-Nevada,* [CD-ROM]. Washington, D.C.: U.S. Geological Survey (Digital Data Series, DDS-55.Version 1.0).

Day, S.J., J.C. Carracedo, H. Guillou, and P. Gravestock, 1999. *Recent structural evolution of the Cumbre Vieja volcano, La Palma, Canary Islands.* J. Volcan. Geotherm. Res. 94, 135-167**.**

Day, S.J., Heleno da Silvab S.I.N., and Fonsecab, J.F.B.D. 1999b. *A past giant lateral collapse and present-day flank instability of Fogo, Cape Verde Islands.* Journal of Volcanology and Geothermal Research, Vol. 94 (1-4) (1999) pp. 191-218.

ElsworthD., and Day S.J. 1999. *Flank collapse triggered by intrusion: the Canarian and Cape Verde Archipelagoes.* Journal of Volcanology and Geothermal Research, Vol. 94 (1-4) (1999) pp. 323-340.

Fritz, H., and Mader C., 2002, *Lituya Bay Mega-Tsunami*. 2nd Tsunami Symposium, Honolulu, Hawaii, USA, May 28-30, 2002.

Furumoto, A. 1966. *Seismicity of Hawaii.* Bulletin of the Seismological Society of America, Feb.

Heleno da Silva, S.I.N. Day S.J. and Fonseca J.F.B.D. 1999. *Fogo Volcano, Cape Verde Islands: seismicity-derived constraints on the mechanism of the 1995 eruption.* Journal of Volcanology and Geothermal Research, Vol. 94 (1-4) (1999) pp. 219-231

Klügela A., Schminckea H.-U, Whiteb J.D.L., and Hoernlea K.A., 1999. *Chronology and volcanology of the 1949 multi-vent rift-zone eruption on La Palma (Canary Islands).* Journal of Volcanology and Geothermal Research, Vol. 94 (1-4) (1999) pp. 267-282.

Kowalik, Z., 2002. *Relationship Between Tsunami Calculations and Physics*. 2nd Tsunami Symposium, Honolulu, Hawaii, USA, May 28-30, 2002.

Lipman, P. W., 1995, *Declining growth of Mauna Loa during the last 100,000 years: Rates of lava accumulation vs. gravitational subsidence: in Mauna Loa Revealed.* Rhodes, J. M., and Lockwood, J. P., American Geophysical Union Geophysical Monograph 92, p. 45-80.

Mader C. L. and Fritz, H. M. 2002, *The Lituya Bay Mega-Tsunami,* 2nd Tsunami Symposium, Honolulu, Hawaii, USA, May 28-30, 2002

Mader C. L., 2001. *Modeling the La Palma Landslide Tsunami.* Science of Tsunami Hazards, Volume 19, pages 150-170 (2001).

Mehl K. W. and Schmincke H.U, 1999. *Structure and emplacement of the Pliocene Roque Nublo debris avalanche deposit, Gran Canaria, Spain.* Journal of Volcanology and Geothermal Research, Vol. 94 (1-4) (1999) pp. 105-134.

Moore, J.G., Clague, D.A., Holcomb, R.T., Lipman, P.W., Normark, W.R., and Torresan, M.E., 1989., *Prodigious submarine landslides on the Hawaiian Ridge.* Journal of Geophysical Research, Series B 12, Volume 94, p. 17,465-17,484. 94, 17,465-17, 484.

McMurtrya G. M., Herrero-Bervera E., Cremera M. D., Smith J. R. , Resig J. , Sherman C. and Torresan M. E., 1999. *Stratigraphic constraints on the timing and emplacement of the Alika 2 giant Hawaiian submarine landslide.* Journal of Volcanology and Geothermal Research, Vol. 94 (1-4) (1999) pp. 35-58.

Moore, J.G., and Chadwick, W.W. Jr., 1995, *Offshore geology of Mauna Loa and adjacent areas, Hawaii.* In Geophysical Monograph 92, Mauna Loa Revealed: structure, composition, history, and hazards, ed. by J.M. Rhodes and J.P. Lockwood, American Geophysical Union, Washington, D.C., p. 21-44.

Moore, J.G., and Clague, D.A., 1992. *Volcano growth and evolution of the island of Hawaii.* Geologic Society of America Bulletin, 104, 1471-1484.

Moore, J.G., Normark, W.R. & Holcomb, R.T., 1994. *Giant Hawaiian Landslides.* Annual Reviews of Earth and Planetary Science, 22, 119-144.

Morgan, J.K., Moore, G.F., and Clague, D.A., 2001, *Papa`u Seamount: the submarine expression of the active Hilina Slump, south flank of Kilauea Volcano, Hawaii.* Journal of Geophysical Research, submitted.

Moss, J.L., McGuire W.J., and Page D. 1999. *Ground deformation monitoring of a potential landslide at La Palma, Canary Islands.* Journal of Volcanology and Geothermal Research, Vol. 94 (1-4) (1999) pp. 251-265.

Pararas-Carayannis, G. , 1976a. *The Earthquake and Tsunami of 29 November 1975 in the Hawaiian Islands.* ITIC Report, 1976.

Pararas-Carayannis, G., 1976b. *In International Tsunami Information Center - A Progress Report For 1974-1976.* Fifth Session of the International Coordination Group for the Tsunami Warning System in the Pacific, Lima, Peru, 23-27 Feb. 1976

Pararas-Carayannis, G and Calebaugh P.J., 1977. *Catalog of Tsunamis in Hawaii, Revised and Updated,* World Data Center A for Solid Earth Geophysics, NOAA, 78 p., March 1977.

Pararas-Carayannis, G, 1988. *Risk Assessment of the Tsunami Hazard*. In Natural and Man-Made Hazards, 1988, D. Reidal, Netherlands, pp.171-181, .

Pararas-Carayannis, G., 1992. *The Tsunami Generated from the Eruption of the Volcano of Santorin in the Bronze Age.* Natural Hazards 5::115-123, Kluwer Academic Publishers. Netherlands.

Pararas-Carayannis, G., 2002. *Volcanically Generated Tsunamis.* 2nd Tsunami Symposium, Honolulu, Hawaii, USA, May 28-30, 2002.

Piper, D.J.W., Shor, A.N. & Hughes Clarke, J.E., 1988. *The 1929 "Grand Banks" earthquake, slump and turbidity current.* Geological Society of America Special Paper 229, 77-92.

Reynolds, J. R., Clague, D.A., Hatcher, G. and Maher, N., 1998. Evolutionary Sequence of Submarine Volcanic Rift zones in Hawaii. *EOS, Transactions American Geophysical Union*, 79, F825.

Rileya C. M. , Diehla, J. F. Kirschvink J. L. andRipperdanc, R. L. 1999. *Paleomagnetic constraints on fault motion in the Hilina Fault System, south flank of Kilauea Volcano, Hawaii.* Journal of Volcanology and Geothermal Research, Vol. 94 (1-4) (1999) pp. 233-249

Shigihara, V., and Imamura, F., 2002. Numerical Simulation Landslide Tsunami 2nd Tsunami Symposium, Honolulu, Hawaii, USA, May 28-30, 2002

Smith, J. R. Malahoff A., and Shor A. N., 1999. *Submarine geology of the Hilina slump and morpho-structural evolution of Kilauea volcano, Hawaii.* Journal of Volcanology and Geothermal Research, V. 94, No 1-4, 1, pp. 59-88 December

Smith W. H. F. and Sandwell D. T, . 1997,. *Global Sea Floor Topography from Satellite Altimetry and Ship Depth Soundings.* Science, April 7, 1997.

Stillman C.J., 1999. *Giant Miocene landslides and the evolution of Fuerteventura, Canary Islands.* Journal of Volcanology and Geothermal Research, Vol. 94 (1-4) (1999)

Ward, S. N., 2001. *Landslide Tsunami*. J. Geophys. Res., Accepted and In Press.

Ward, S. N. and S. Day 2001. *Cumbre Vieja Volcano -- Potential Collapse and Tsunami at La Palma, Canary Islands*. Geophys. Res. Lett. , Submitted.

Weaver, R., G. Gisler, G., and M. Gittings, 2002. *Asteroid Generated Tsunamis.* 2nd Tsunami Symposium, Honolulu, Hawaii, USA, May 28-30, 2002

Walker George P.L., 1999. *Volcanic rift zones and their intrusion swarms.* Journal of Volcanology and Geothermal Research, Vol. 94 (1-4) (1999) pp. 21-34

White J. D.L. and Schmincke H-U., 1999. *Phreatomagmatic eruptive and depositional processes during the 1949 eruption on La Palma (Canary Islands).* Journal of Volcanology and Geothermal Research, Vol. 94 (1-4) (1999) pp. 283-304

AN EXPERIMENTAL STUDY OF TSUNAMI RUNUP ON DRY AND WET HORIZONTAL COASTLINES

Hubert CHANSON
Dept. of Civil Engineering, The University of Queensland, Brisbane QLD 4072, Australia ([1])
Fax : (61 7) 33 65 45 99 - Email : h.chanson@mailbox.uq.edu.au

Shin-ichi AOKI,
and
Mamoru MARUYAMA
Dept. of Architecture and Civil Engineering, Toyohashi University of Technology, Toyohashi, 441- 8580, Japan

ABSTRACT

Wave runup generated by a tsunami reaching the shoreline may induce devastating flood waves. When tsunami wave breaking is associated with a plunging jet, some energy dissipation at jet impact and the downstream propagation of the surge is characterised by a high initial momentum resulting from the plunging jet. New experiments were performed in a large-size facility (15-m long 0.8-m wide channel). The experimental data highlight a large wave celerity during the initial stage (i.e. $x/d_0 < 10$), followed by some deceleration caused by bottom friction and turbulent energy dissipation. The wave front travels faster than a 'classical' dam break wave because of the higher momentum of the wave. Further downstream (i.e. $x/d_0 > 30$), the bore propagates at a speed similar to that predicted by the 'classical' analysis. The results highlight a reduced warning time downstream of plunging breaking wave.

[1]Author to whom the correspondence should be adressed.

1. Introduction

1.1 Presentation

A tsunami is a long-period wave generated by ocean bottom motion during an earthquake with wave length of about 200 to 350 km. Although the wave amplitude is moderate in deep waters (e.g. 0.5 to 1 m), the tsunami wave slows down and the wave height increases near the shoreline until it breaks. The wave runup height might reach several metres above the natural sea level and cause significant damage. Major tsunami disasters were associated with well in excess of 140,000 losses of life (e.g. YEH et al. 1996, HEBENSTREIT 1997, CHANSON et al. 2000). Figure 1 shows a warning sign post along a road to the Enshu coastline, Japan. This shoreline has been historically affected by severe tsunamis. For example, the mouth of the Hamanako lake was drastically altered by a tsunami in AD 1498 (Earthquake magn. 8.6). The estuary mouth shifted by about 3.5 km and the previously freshwater lake became a saltwater system.
When the tsunami wave is slowed down by dry bed friction and overturns, the propagation of the bore on the shore is somewhat similar to the wave propagation downstream of a free-falling jet impact. For example, MURCK et al. (1997) described that Vajont dam overtopping wave as a "*tsunami-like wave*". A dominant feature of the advancing bore is its high initial momentum resulting from the breaker plunging jet. When the coastline is flat, the abnormal rise of sea level associated with the tsunami wave may runup across flat lands, sweeping away buildings and carrying ships inland. In two documented cases, the runup occurred over lakes and lagoon : i.e., at Gargano (Italy) on 30 July 1637 and at the Sissano Lagoon (PNG) on 17 July 1998 when more than 8,000 lives were lost altogether (BUTCHER et al. 1994, SARRE 1998).

Fig. 1 - Road sign post warning of tsunami danger - Takatoyo beach on the Enshu coast, Toyohashi, Japan

1.2 Analogy with dam break wave on dry and wet channels

Considering an ideal dam break surging over a dry river bed (Fig. 2A), the method of characteristics may be applied to solve completely the wave profile (e.g. HENDERSON 1966, MONTES 1998). For a horizontal rectangular channel, the shape of the ideal surge free-surface satisfies :

$$\frac{x}{t} = 3 * \sqrt{g * d} - 2 * \sqrt{g * d_o} \quad (1)$$

where the longitudinal origin (x = 0) is the dam location, t is the time, the time origin (t = 0) is the instantaneous dam break, d is the flow depth and d_o is the initial reservoir water depth (Fig. 2A). After dam break, the flow depth and discharge at the origin x = 0 are constants :

$$d_{(x=0)} = \frac{4}{9} * d_o \quad (2)$$

$$Q_{(x=0)} = \frac{8}{27} * d_o * \sqrt{g * d_o} * B \quad (3)$$

and the celerity of the wave front equals :

$$C_S = 2 * \sqrt{g * d_o} \qquad (4)$$

Fig. 2 - Definition sketches
(A) Dam break wave propagation over dry channel
(B) Dam break wave propagation in a channel with an initial water depth

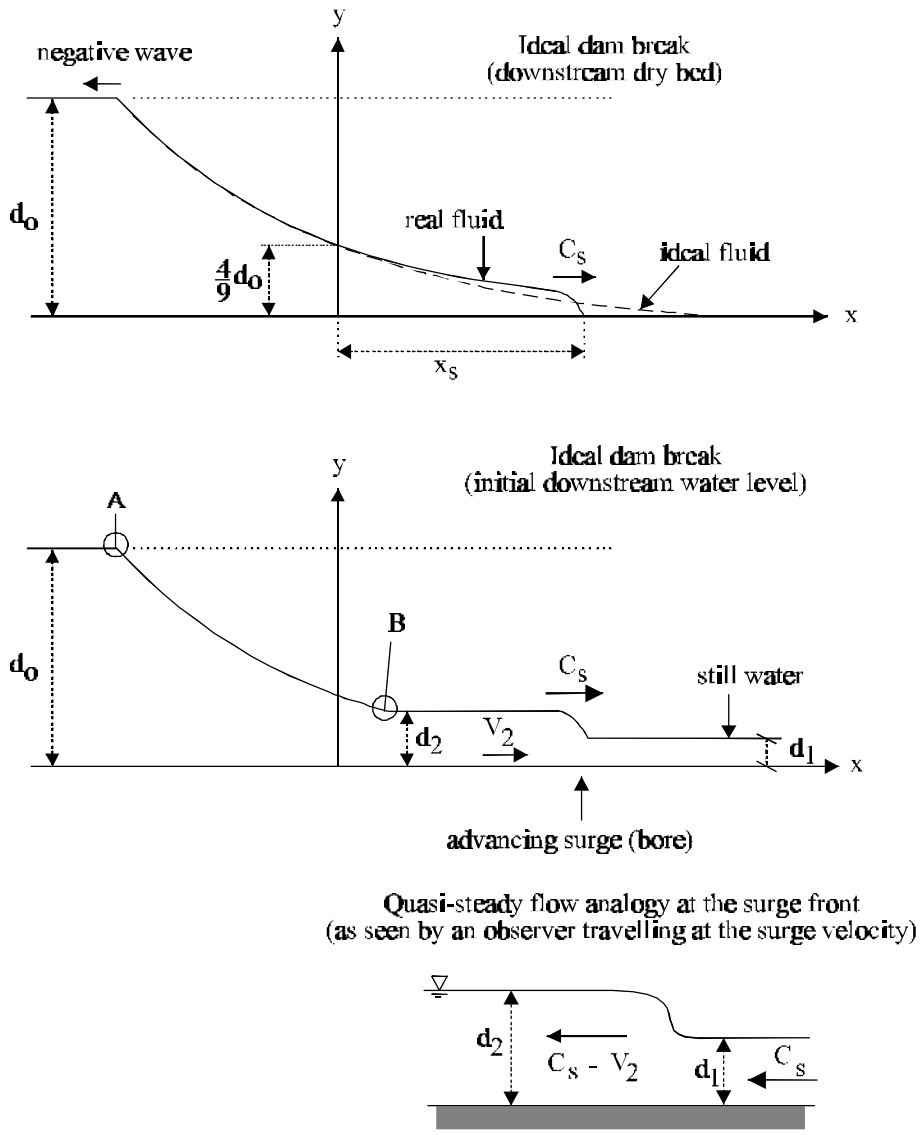

Although Equations (1) to (4) assume no boundary friction, model and prototype experiments showed good agreement with the theory, but for the leading edge of the wave (i.e. Eq. (4)). Bottom friction affects significantly the propagation of the leading tip and, taking into account the flow resistance, WHITHAM (1955) developed an analogy between the wave front and a turbulent boundary layer. For a horizontal dry channel, his estimate of the wave front celerity is best correlated by :

$$\frac{C_s}{\sqrt{g*d_o}} = \frac{2}{1.0 + 2.807 * \left(\frac{f}{8} * \sqrt{\frac{g * t^2}{d_o}}\right)^{0.425}} \quad (5)$$

with a normalised coefficient of correlation of 0.999973 and where f is the Darcy friction factor. WHITHAM (1955) commented that his work was applicable only for $C_s/\sqrt{g*d_o} > 2/3$.

The propagation of a dam break wave over still water (initial depth $d_1 > 0$) is a different situation because the dam break wave is lead by a positive surge (Fig. 2B) (HENDERSON 1966). The basic flow equations are the continuity and momentum equation across the positive surge front, and the condition along the characteristics. The system of equation may be solved graphically as (MONTES 1998) :

$$\sqrt{\frac{d_o}{d_1}} = \frac{1}{2} * \frac{C_s}{\sqrt{g * d_1}} * \left(1 - \frac{1}{X}\right) + \sqrt{X} \quad (6)$$

where

$$X = \frac{1}{2} * \left(\sqrt{1 + 8 * \frac{C_s^2}{g * d_1}} - 1\right) \quad (7)$$

Equation (6) may be correlated by ;

$$\frac{C_s}{\sqrt{g*d_1}} = \frac{0.63545 + 0.3286*\left(\frac{d_1}{d_o}\right)^{0.65167}}{0.00251 + \left(\frac{d_1}{d_o}\right)^{0.65167}} \quad (8)$$

with a normalised coefficient of correlation of 0.9999996. The flow depth downstream of (behind) the positive surge is deduced from the continuity and momentum equations (HENDERSON 1966, CHANSON 1999).

1.3 Physical modelling of tsunami wave runup

In a physical model, the flow conditions are said to be similar to those in the prototype if the model displays similarity of form, similarity of motion and similarity of forces. For free-surface flow studies, including tsunami wave runup and dam break wave, the gravity effect is usually predominant, and model-prototype similarity is performed with a Froude similitude (e.g. FAURE and NAHAS 1965, IPPEN 1966, HUGHES 1993). If the same fluids are used in both model and prototype, distortions are introduced by effects other than gravity (e.g. viscosity, surface tension) resulting in scale effects.

Considering a tsunami wave runup, bed friction opposes the fluid motion. The modelling of flow resistance is not a simple matter and often the geometric similarity of roughness height and spacing is not enough (HENDERSON 1966, CHANSON 1999). For an undistorted model, a Froude similitude implies that the model flow resistance will be similar to that in prototype if the following condition is satisfied :

$$f_R = \frac{f_p}{f_m} = 1 \quad (9)$$

where f is the Darcy friction factor, the subscripts p and m refer respectively to prototype and model flow conditions, while the subscript R refers to the ratio of prototype to model characteristics. Most prototype flows are turbulent and the model flow conditions must be turbulent : i.e., $Re_m > 5000$ to 10000 where Re is the Reynolds number.

Prototype wave runup is further characterised by significant air entrainment ('white waters') at the wave front (e.g. Fig. 4A). It is recognised that scale effects in terms of air bubble entrainment may take place with

a Froude similitude for L_R > 10 to 20, or L_R < 0.05 to 0.1 where L_R is the geometric scaling ratio (e.g. WOOD 1991, CHANSON 1997). Near the shoreline, breaking waves contribute to set sediment matters into suspension. The strong turbulent mixing, observed in the laboratory and in the field, is further enhanced by the upwelling circulation induced by the rising air bubbles. Subsequently, the combined effects of jet mixing and rising bubbles have a direct impact on the sediment transport processes (e.g. NIELSEN 1984). Physical modelling of the three-phase flow is practically impossible, but at full-scale.
Dam break wave and tsunami runup carries inland sediment materials and debris. The primary difficulty with movable-bed hydraulic models is the scaling of both the sediment movement and the fluid motion. Further the bed roughness becomes a function of the bed geometry and of the sediment transport. Several authors (e.g. HENDERSON 1996, pp. 497-508, GRAF 1971, pp. 392-398) discussed methods for 'designing' a movable bed model. CHANSON (1999, pp. 301-304) presented a detailed analysis of sediment transport modelling.

In summary, the physical modelling of tsunami wave runup in shallow waters and over dry land is very complex. In the present study, the authors investigate the wave propagation downstream of plunging jet impact in a large-size facility to minimise potential scale effects. New experiments were performed in a horizontal rectangular channel with the channel being initially dry or filled with a known water depth. The results provide new information on the energy dissipation at jet impact and on the downstream wave propagation.

2. Experimental configuration

An experimental study of wave runup downstream of plunging jet impact was conducted in a 15-m long 0.8-m wide 0.65-m deep channel (Fig. 3). The flume was horizontal and made of newly painted steel and some glass sidewall panels. The surge wave was generated by the vertical release of a known water volume through a rectangular, sharp-crested orifice (70-mm by 750 mm) at one end of the channel. A 0.5-m high sloping beach (1V:6H) was installed at the other end. The hydrograph of the free-falling jet was deduced from continuous water level measurements in the reservoir. The relationship between the tank volume and free-surface level was calibrated in-situ and the water level was measured with a capacitance wave gauge. The surging flow in the channel was studied with two video-cameras : a VHS-C camescope National™ CCD AG-30C (speed: 30 frames/sec., shutter: 1/60 & 1/1,000 sec.) and a digital handycam Sony™ DV-CCD DCR-TRV900 (speed: 30 frames/sec., shutter: 1/4 to 1/10,000 sec., zoom: 1 to 48). One camera was installed above and along the axis of the channel while the second took sideview pictures of the wave front through glass sidewall panels. Note that sideview pictures were difficult to analyse for small wave heights.

Table 1 - Summary of the experiments

Run No.	Initial volume	Head above orifice H_1	Fall height orifice-bed h	Initial water level in channel d_1	Initial discharge Q	Remarks
	m^3	m	m	m	m^3/s	
(1)	(2)	(3)	(4)	(5)	(6)	(7)
1	0.907	0.653	1.330	0.0 (*)	0.117	Run 990416_1.
2	1.031	0.740	1.330	0.0 (*)	0.124	Run 990420_1.
3	1.031	0.740	1.330	0.030	0.124	Run 990421_1.
4a	1.076	0.771	1.324	0.199	0.129	Run 990531_1.
4b	0.790	0.570	1.324	0.200	0.111	Run 990531_2.
4c	0.452	0.328	1.324	0.201	0.087	Run 990531_3.

Note : (*) : initially wet channel bed.

Fig. 3 - Experimental facility
(A) Sketch of the experiment

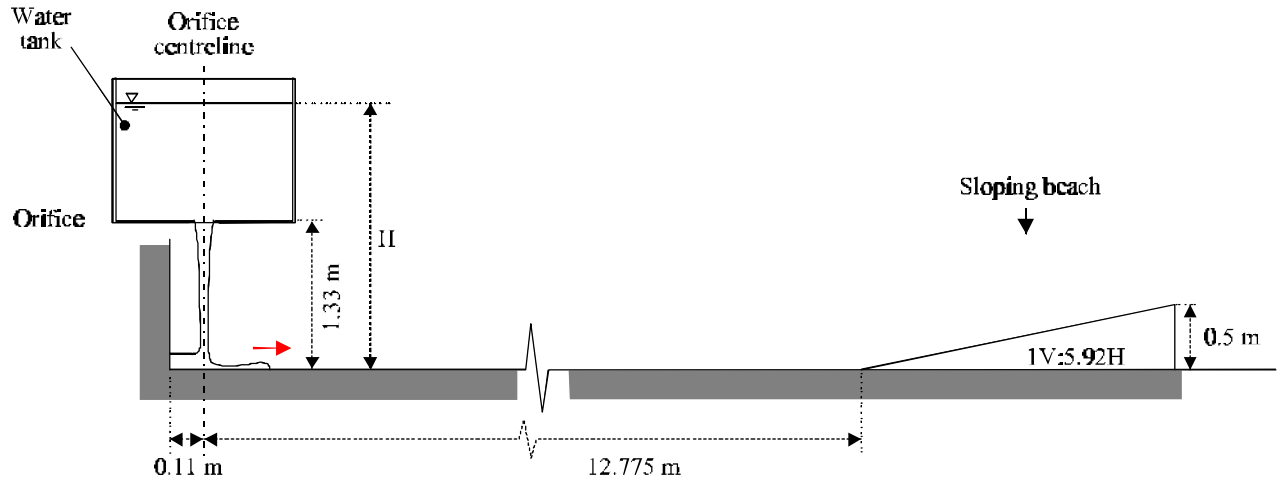

(B) Top view of the flume, with the circular water reservoir on the right of the photograph

Prior to the start of each experiment, the reservoir was filled with a known volume of water (Table 1, column 2), the orifice gate being shut. The channel was initially either dry or filled with a known water depth d_1 (Table 1, column 5). The orifice opening occurred in less than 30 milliseconds and the free-falling jet took about 260 milliseconds to reach the channel invert. The time origin (t = 0) was taken as the time of jet impact onto the channel invert or channel free-surface. The longitudinal origin (x = 0) was at the centreline of the jet. The error on the time was about 1/30 s, the error on the water depth was about +/- 1 cm and the error on the longitudinal position was +/- 2 cm. Further details on the experimental investigations were reported in CHANSON et al. (2000, 2002).
Six flow conditions were carefully documented (Table 1). In addition qualitative observations were conducted during a number of tests with initial water levels d_1 = 0 (dry channel), 0.015 and 0.3 m.

3. Experimental results

3.1 Flow patterns

Considering one single experiment, a typical sequence of events included the rapid opening of the water tank, the free-falling jet, nappe impact into the flume, the propagation of the flood wave, wave runup on the sloping beach and reflection of the wave front. Figure 4 presents typical photographs of the wave runup.

Immediately after gate opening, the free-falling jet impacted onto the channel bed or the water free-surface if the channel was initially filled with water. The initial impact was characterised by a lot of splashing and the formation of waves. (The leading wave was a positive surge when the channel was initially filled with water.) The jet impact was associated with significant energy dissipation. : i.e., the observed rate of energy dissipation ranged between 70 and 90%. The estimate was difficult because of the high level of turbulence of the surge as well as the existence of a wave front reflection on the solid boundary located at x = - 0.11 m. Following the jet impact, a wave front developed and travelled towards the downstream end of the channel (i.e. sloping beach). The wave front appeared highly aerated (e.g. Fig. 4A) for all the investigations (i.e. both $d_1 = 0$ and $d_1 > 0$). Once the wave front reached the beach, it was reflected and travelled back to the other channel end. The wave front propagation was recorded until the wave front was barely perceptible with video-camera pictures.

Fig. 4 - Wave propagation in the channel - Run No. 3, $d_1 = 0.03$ m
(A)Wave propagation (t ~ 3.5 s, x_s ~ 8 m)

(B) Wave runup on the slope beach surging to overflow the beach crest (t ~ 6 s)

3.2 Wave propagation

Figure 5 shows typical surge front data measured from the side window ($3.2 \leq x \leq 4.1$ m). The figure presents data for the first bore and the reflected bores. The horizontal time scale is in 1/30 s. For the first wave, the observed wave front shape was in agreement with the experimental data of SCHOKLITSCH (1917), FAURE and NAHAS (1961) and LAUBER (1997).

Wave front propagation speeds are presented in Figure 6. Figure 6A shows C_s/V_i where C_s is the horizontal wave front celerity and V_i is the initial jet impact velocity : i.e., $V_i = \sqrt{2*g*(H_1+h)}$. At any time $t > 0$, the jet impact velocity equals $\sqrt{2*g*(H+h)}$ where H is the total head above orifice. For $t \leq 0$, $H = H_1$. C_s was deduced from the derivative $\partial x_s/\partial t$ of the best curve fit of the data (x_s, t) where x_s is the horizontal distance between the origin and the wave front, and t is the time. The data suggest a strong deceleration in the first part of the runup up to $x/d_o = 20$ to 30, where d_o is a measure of the initial flow rate :

$$d_o = \frac{9}{4} * \sqrt[3]{\frac{Q^2}{g * B^2}} \qquad (2)$$

Q is the initial discharge (i.e. t = 0+) and B is the channel breadth. For an ideal dam break, d_o would be equivalent to the initial water level and Q would be the discharge at the origin. The present results indicate that boundary friction is significant in the first part of the horizontal runup (i.e. $x/d_o > 25$). For $x/d_o > 30$, friction losses became smaller and the wave front celerity decayed gradually. Figures 6B and 6C presents the dimensionless wave celerity $C_s/\sqrt{g*d_o}$ as a function of the dimensionless distance x/d_o. The results

show that $C_s/\sqrt{g*d_o}$ ranged from 3 down to 0.8. That is, it was significantly larger than the celerity of a dam break wave, particularly for $x/d_o < 25$.

Fig. 5 - Shape of the wave front ($x \approx 3.5$ m)
Experiment No. 3, Initial water level : $d_1 = 0.03$ m

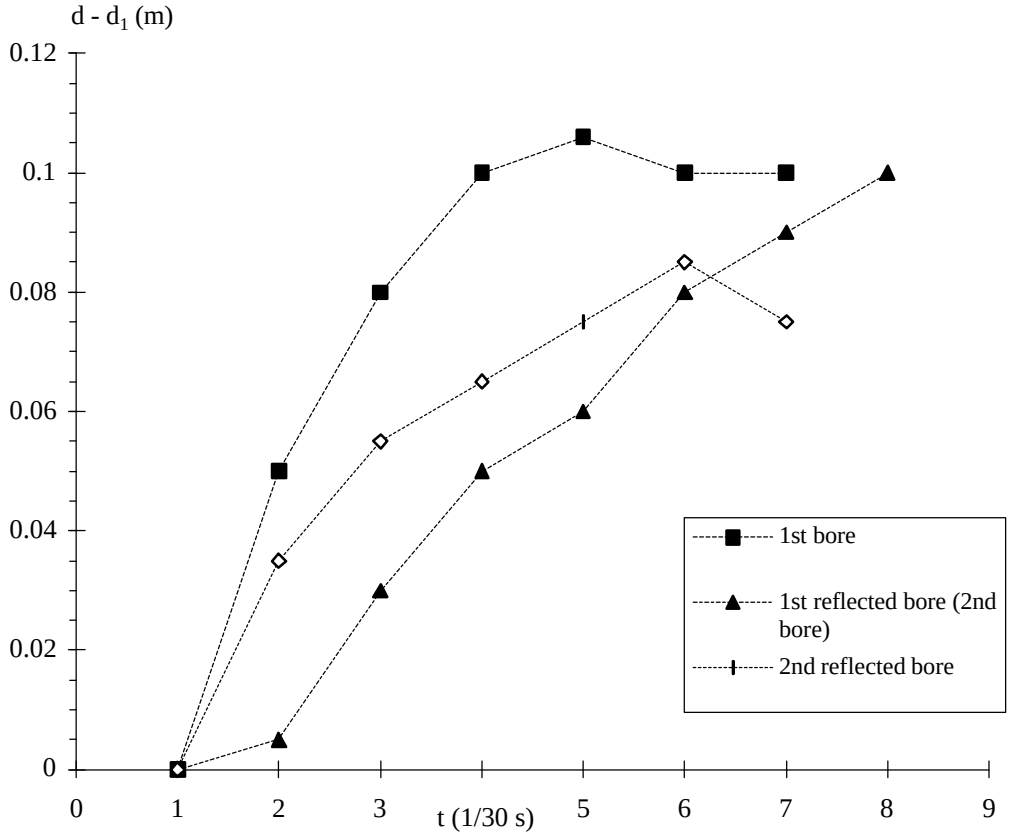

For an initial dry channel, the data (Fig. 6B) show consistently a greater wave front celerity than for the dam break analysis (WHITHAM's solution) for $x/d_o < 25$. Close to the jet impact, the wave celerity was found to be nearly twice that of the classical dam break wave (Fig. 6B). A main difference was the larger initial momentum of the wave during the present study despite significant energy loss at jet impact. The experimental data imply further a strong deceleration up to $x/d_o = 25$ to 30 (Fig. 6B). Practically the experimental data for an initially dry channel are best correlated by :

$$\frac{C_s}{V_i} = \frac{0.598}{1 - 0.0336 * \frac{x}{d_o} + 0.00237 * \left(\frac{x}{d_o}\right)^2} \quad \text{Initial dry horizontal channel } (4 < x/d_o < 30) \quad (10)$$

where V_i is the initial jet impact velocity. For $x/d_o > 30$, the agreement between the data and WHITHAM's solution is fair.

For a channel initially filled with water (Fig. 6C), the data compared favourably with the application of the momentum principle to a positive surge (HENDERSON 1966, CHANSON 1999). The results (Fig. 6C) indicated a slightly greater wave front celerity up to $x/d_o = 20$ to 25. Further downstream, the present data were consistent with the application of the momentum principle. As a first estimate, the data were best correlated by:

Fig. 6 - Propagation of the wave front

(A) C_s/V_i - Comparison with Equations (10) and (11) for dry channel and initially-filled channel respectively

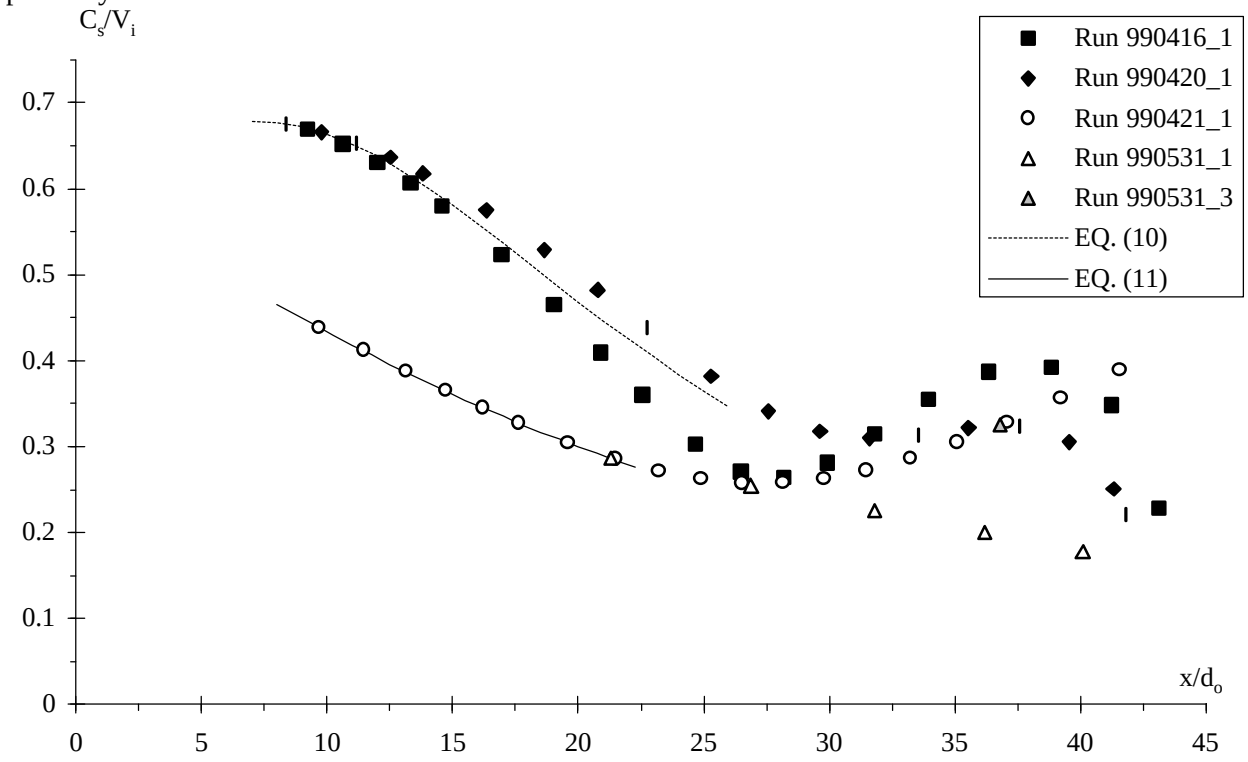

(B) $C(s)/\sqrt{g*d_o}$ (dry channel bed $d_1 = 0$) - Comparison with WHITHAM's (1955) theory

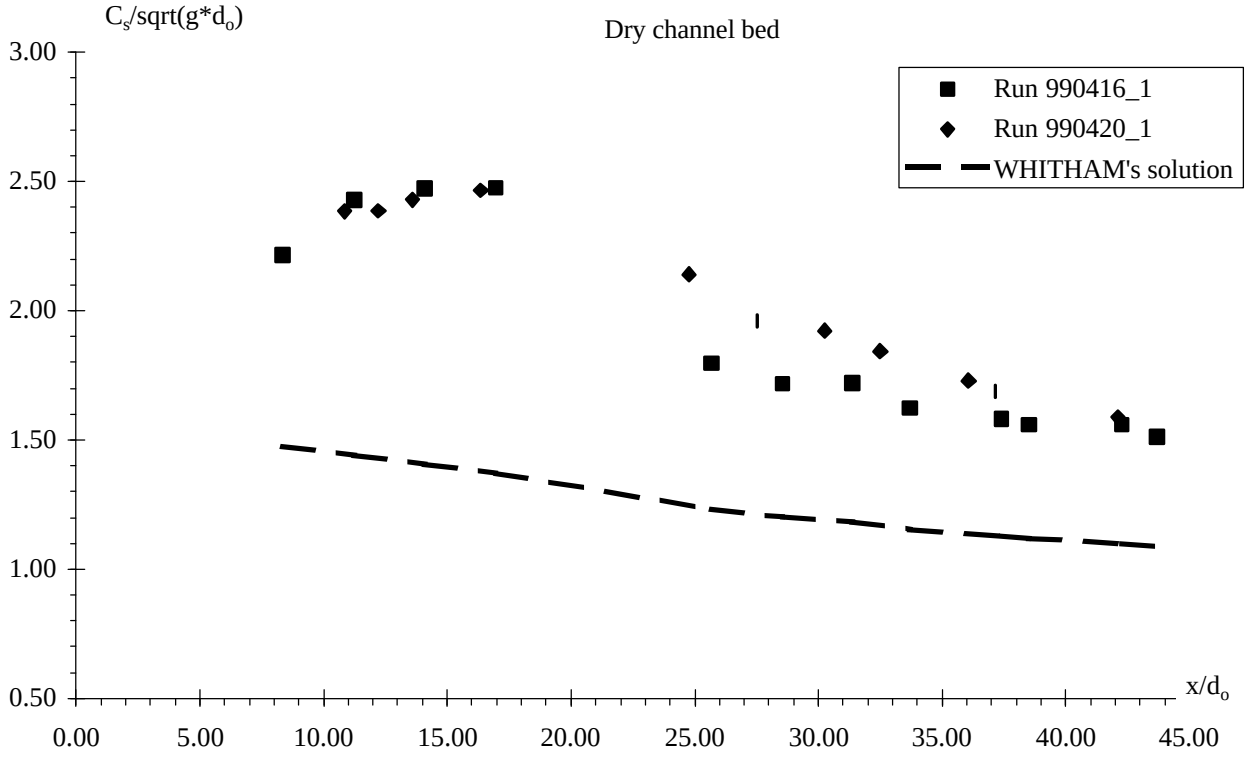

(C) C(s)/$\sqrt{g*d_o}$ (initial water depth $d_1 > 0$) - Comparison with the momentum principle

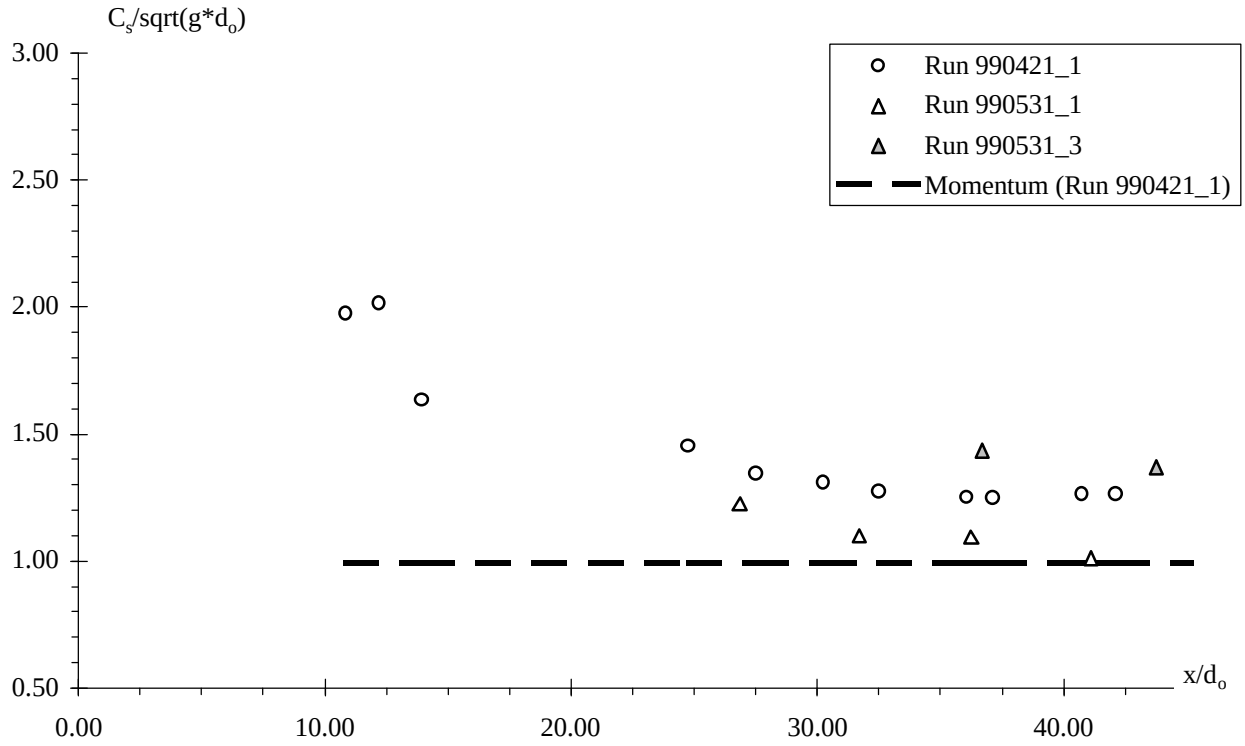

$$\frac{C_s}{V_i} = \frac{0.598}{1 + 0.0263 * \frac{x}{d_o} + 0.00117 * \left(\frac{x}{d_o}\right)^2} \qquad (0.1 < d_1/d_o < 0.8 \text{ and } 10 < x/d_o < 25) \quad (11)$$

Note that the result is little affected by the initial water depth within the range $0.1 < d_1/d_o < 0.8$.
Both Equations (10) and (11) are compared with the data in Figure 6A.

3.3 Wave runup height

The maximum runup height on the sloping beach was recorded (Table 2). For a dry channel, the initial wave runup height H_r reached about

$$\frac{H_r}{H_1 + h} \approx 0.215 \qquad (12)$$

where H_1 is the head above orifice and h is the fall height between the orifice and the channel bed. For a given experiment, the data show a decrease in the subsequent runup heights from the first (initial) bore until the third one. Once the bore become an undular surge, the energy loss is drastically reduced and the decay in runup height becomes significantly smaller.
For a channel initially filled with water, the beach was overtopped at the first runup (i.e. $H_r/(H_1+h) > 0.3$) for all investigated initial water depths, including for the smallest water depth $d_1 = 0.015$ m. The overtopping event lasted typically about 1 +/- 0.1 seconds.

Comparison with wave runup height on beaches
For non-breaking waves, the linear wave theory predicts a maximum runup height of :

$$\frac{H_r}{a} = \sqrt{\frac{2 * \pi}{\theta}} \qquad \text{Non-breaking wave (13)}$$

where a is the amplitude of the wave and θ is the beach slope in radian. For a 1:5.7 beach slope (LI and RAICHLEN 2002), the wave runup height of a solitary wave was about :

$$\frac{H_r}{d_1} \approx 3.09 * \left(\frac{H_b}{d_1}\right)^{0.95} \qquad \text{Breaking solitary wave (14)}$$

where H_b is the wave breaking height. For breaking waves, the runup height of a "surging bore" equals :

$$H_r = \frac{C_s^2}{2 * g} \qquad \text{Breaking wave (surge) (15)}$$

where C_S is the horizontal component of the bore celerity as it reaches the shore (e.g. LE MEHAUTE et al. 1968). Equation (15) would predict, within 20%, the observed runup height for the experiments with initial dry channel bed, using the observed wave front celerity. [This assumption is consistent with observations of horizontal velocity component at wave breaking by CHANSON and LEE (1997).] The same calculations (Eq. (15)) would however underestimate greatly the runup height for each experiment with initial non-zero water depth. It is suggested that the runup wave heights recorded during the present study were greater because of the high initial horizontal momentum of the bore.

Table 3-2 - Maximum surge runup height data on the sloping beach (experimental observations)

Run No.	Initial water level in channel d_1 m	Initial discharge Q m3/s	Runup height H_r m	Remarks
(1)	(2)	(3)	(4)	(5)
1	0.000	0.117	0.43	First runup.
			0.17	Second runup.
			0.11	Third runup. Undular bore.
2	0.000	0.124	0.443	First runup.
			0.17	Second runup.
			0.15	Third runup.
			0.15	Fourth runup. Undular bore.
3	0.030	0.124	> 0.5	First runup. beach overtopping for 0.9 sec.
			0.216	Second runup.
4a	0.199	0.129	> 0.5	First runup. Beach overtopping for 0.9 sec.
			> 0.5	Second runup. Beach overtopping for 1.1 sec.

4. Applications

Overall the present study shows consistently a larger wave celerity downstream of jet impact compared to a classical dam break wave. Relevant application include tsunami runup downstream of plunging breaking waves and wave runup downstream of an overtopped dam (Fig. 7). Dam overtopping may be caused by impulse waves generated by rockfalls, landslides, ice falls, glacier breakup or snow avalanches in the reservoir (e.g. Vajont dam catastrophe). Some impulse waves might be induced by earthquake-generated falls. VISCHER and HAGER (1998) gave a thorough summary of the hydraulics of impulse waves. Another cause of dam overtopping is the sudden overtopping of fully-silted reservoirs by tropical storm runoff. In South-East Australia, CHANSON and JAMES (1999) documented such fully-silted dams which are safety hazards.

For any application, the present results imply that the warning time of wave arrival is significantly smaller downstream of a falling jet than that predicted by a classical dam break wave theory.
Considering a tsunami wave (0.15 m high) generated in deep water (1000 m), the wave will break near the shore for d = 8.2 m and a wave height of 5.8 m (CHANSON et al. 2000). Assuming a plunging breaking wave, the resulting "bore" would propagate inland and Equation (10) would predict that the wave would take about 35 seconds to reach a point located 300-m from the shoreline (for a dry horizontal shore). For a bore travelling over a wet land (1-m water depth), the surge would take about 50 seconds to progress 300-m inland. Note that the latter calculations are not strictly correct because the tsunami runup was approximated by a turbulent surge while Equation (11) was deduced from experiments corresponding to a pseudo-plunging breaker.

Fig. 7 - Applications

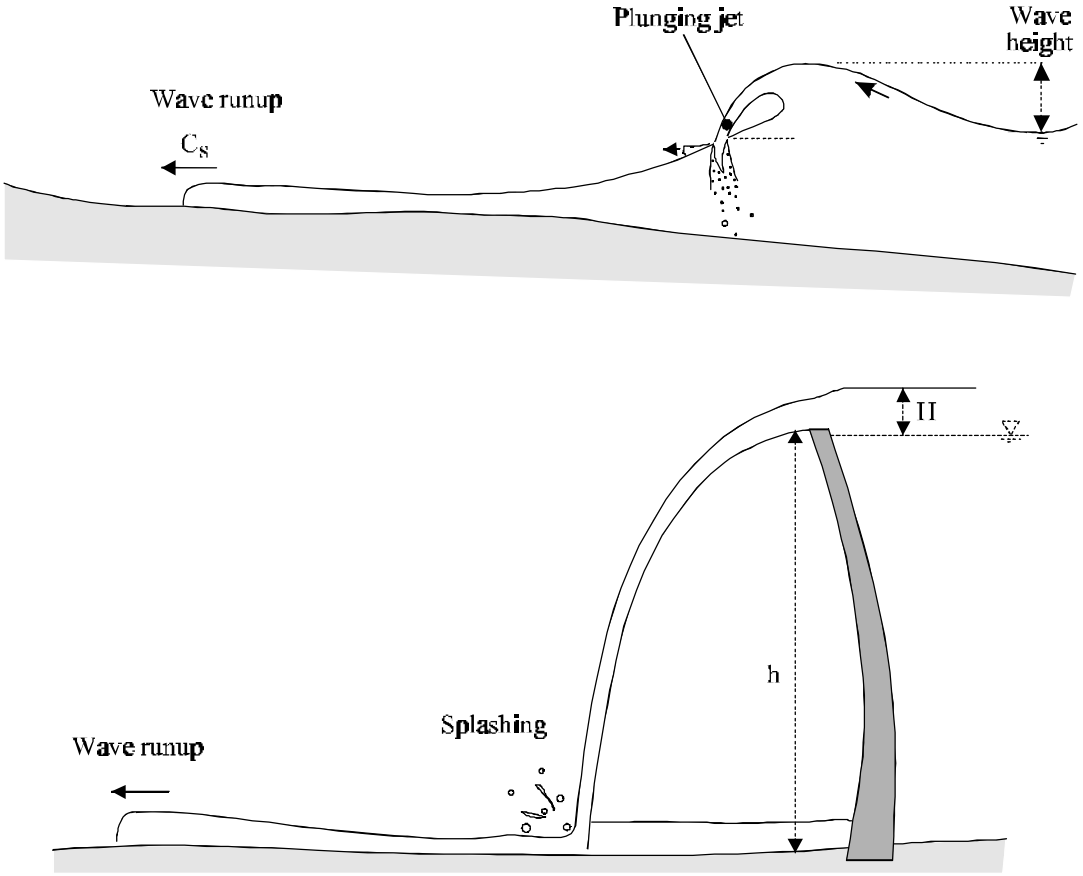

5. Summary and conclusions

This study investigates the horizontal runup of waves (i.e. bores) downstream of a free-falling jet in a large-size facility. The dominant characteristics of the advancing wave is its high initial momentum and, as a result, the wave front usually travels faster than a 'classical' dam break wave. The experimental data highlight the large wave celerity during the initial stage (i.e. $x/d_o < 10$), followed by some deceleration caused by bottom friction and turbulent energy dissipation. Further downstream (i.e. $x/d_o > 30$), the bore propagates at a speed similar to that predicted by a 'classical' analysis. New correlations (Eq. (10) and (11)) were presented to estimate roughly the wave celerity for $x/d_o < 20$ to 25.
Overall the experimental results highlight the rapid wave propagation downstream of plunging breaking waves and free-falling jets (Fig. 7). The larger wave celerity implies shorter warning times, compared to

classical dam break analysis. Further experimental work should investigate systematically the characteristics of the wave runup.

Acknowledgments

The authors acknowledge the financial support of the Australian Academy of Science, Japan Society for the Promotion of Science and Ministry of Education, Japan.

Notation

The following symbols are used in this report :

a	wave amplitude (m);
B	channel width (m);
C_s	wave front velocity (m/s);
d	water depth (m);
d_o	equivalent dam break reservoir depth (m) : $d_o = \frac{9}{4} * \sqrt[3]{\frac{Q^2}{g * B^2}}$
d_1	initial water depth (m) in the channel;
Fr	Froude number;
f	Darcy-Weisbach friction factor;
g	gravity constant (m/s^2);
H	total head above orifice (m);
H_b	breaking wave height (m);
H_r	wave runup height (m) on sloping beach;
H_1	initial total head above orifice (m);
h	fall height (m) measured from the orifice down to the channel bed;
L	length (m);
Q	total volume discharge (m^3/s) of water;
Re	Reynolds number;
t	time (s);
V	velocity (m/s);
V_i	initial jet impact velocity (m/s): $V_i = \sqrt{2*g*(H_1+h)}$;
X	dimensionless parameter;
x	horizontal longitudinal Cartesian co-ordinate (m); x = 0 at orifice centreline;
x_s	wave front coordinate (m);

Greek symbols

μ	water dynamic viscosity (Pa.s);
ν	water kinematic viscosity (m^2/s) : $\nu = \mu/\rho$;
π	π = 3.14159265358979323846264 3;
ρ	water density (kg/m^3);
$\varnothing$	diameter (m);

Subscript

R	ratio of prototype to model characteristics;
m	model;
p	prototype;
1	initial flow conditions.

References

BUTCHER, G.W., BEETHAM, R.D., MILLAR, P.J., and TANAKA, H. (1994). "The Hokkaido-Nansei-Oki Earthquake. Final Report of the NZNSEE Reconnaissance Team." *Bulletin of the New Zealand Society for Earthquake Engineering*, Vol. 27, No. 1, p. 2.

CHANSON, H. (1997). "Air Bubble Entrainment in Free-Surface Turbulent Shear Flows." *Academic Press*, London, UK, 401 pages.

CHANSON, H. (1999). "The Hydraulics of Open Channel Flows : An Introduction." *Butterworth-Heinemann*, Oxford, UK, 512 pages.

CHANSON, H., AOKI, S., and MARUYAMA, M. (2000). "Experimental Investigations of Wave Runup Downstream of Nappe Impact. Applications to Flood Wave Resulting from Dam Overtopping and Tsunami Wave Runup." *Coastal/Ocean Engineering Report*, No. COE00-2, Dept. of Architecture and Civil Eng., Toyohashi University of Technology, Japan, 38 pages.

CHANSON, H., AOKI, S., and MARUYAMA, M. (2002). "Unsteady Two-Dimensional Orifice Flow: a Large-Size Experimental Investigation." *Jl of Hyd. Res.*, IAHR, Vol. 40, No. 1, pp. 63-71.

CHANSON, H., and JAMES, D.P. (1999). "Siltation of Australian Reservoirs : some Observations and Dam Safety Implications." *Proc. 28th IAHR Congress*, Graz, Austria, Session B5, 6 pages.

CHANSON, H., and LEE, J.F. (1997). "Plunging Jet Characteristics of Plunging Breakers." *Coastal Engineering*, Vol. 31, No. 1-4, July, pp. 125-141.

FAURE, J., and NAHAS, N. (1961). "Etude Numérique et Expérimentale d'Intumescences à Forte Courbure du Front." ('A Numerical and Experimental Study of Steep-Fronted Solitary Waves.') *Jl La Houille Blanche*, No. 5, pp. 576-586. Discussion: No. 5, p. 587.

FAURE, J., and NAHAS, N. (1965). "Comparaison entre Observations Réelles, Calcul, Etudes sur Modèles Distordu ou Non, de la Propagation d'une Onde de Submersion." ('Comparison between Field Observations, Calculations, Distorted and Undistorted Model Studies of a Dam Break Wave.') *Proc. 11th IAHR Biennial Congress*, Leningrad, Russia, Vol. III, Paper 3.5, pp. 1-7 (in French).

GRAF, W.H. (1971). "Hydraulics of Sediment Transport". *McGraw-Hill*, New York, USA.

HEBENSTREIT, G. (1997). "Perspectives on Tsunami Hazard Reduction. Observations, Theory and Planning." *Kluwer Academic*, Dordrecht, the Netherlands, 218 pages. (also *Proc. 17th Intl Tsunami Symp.*, AGU, Boulder CO, USA, July 1995.)

HENDERSON, F.M. (1966). "Open Channel Flow." *MacMillan Company*, New York, USA.

HUGHES, S.A. (1993). "Physical Models and Laboratory Techniques in Coastal Engineering." *Advanced Series on Ocean Eng.*, Vol. 7, World Scientific Publ., Singapore.

IPPEN, A.T. (1966). "Estuary and Coastal Hydrodynamics." *McGraw-Hill*, New York, USA.

LAUBER, G. (1997). "Experimente zur Talsperrenbruchwelle im glatten geneigten Rechteckkanal." ('Dam Break Wave Experiments in Rectangular Channels.') *Ph.D. thesis*, VAW-ETH, Zürich, Switzerland (in German). (also *Mitteilungen der Versuchsanstalt fur Wasserbau, Hydrologie und Glaziologie*, ETH-Zurich, Switzerland, No. 152).

LE MEHAUTE, B., KOH, R.C., and HWANG, L.S. (1968). "A Synthesis on Wave Run-up." *Jl of Waterways and Harbors Div.*, Proceedings, ASCE, Vol. 4, No. WW1, pp. 77-92.

LI, Y., and RAICHLEN, F. (2002). "Non-Breaking and Breaking Solitary Wave Run-up". *Jl of Fluid Mech.*, Vol. 456, pp. 295-318.

MONTES, J.S. (1998). "Hydraulics of Open Channel Flow." *ASCE Press*, New-York, USA, 697 pages.

MURCK, B.W., SKINNER, B.J., and PORTER, S.C. (1997). "Dangerous Earth. An Introduction to Geologic Hazards." *John Wiley*, New York, USA, 300 pages.

NIELSEN, P. (1984). "Field Measurements of Time-Averaged Suspended Sediment Concentrations under Waves." *Coastal Engineering*, Vol. 8, pp. 51-72.

SARRE (1998?). "Calculating the Threat of a Tsunami." *Australian Academy of Science Nova Internet paper* {Internet address : http://www.science.org.au/nova/045/045key.htm}.

SCHOKLITSCH, A. (1917). Über Dambruchwellen." *Sitzungberichten der Königliche Akademie der Wissenschaften, Vienna*, Vol. 126, Part IIa, pp. 1489-1514.

VISCHER, D., and HAGER, W.H. (1998). "Dam Hydraulics." *John Wiley*, Chichester, UK, 316 pages.

WITHAM, G.B. (1955). "The Effects of Hydraulic Resistance in the Dam-Break Problem." *Proc. Roy. Soc. of London*, Ser. A, Vol. 227, pp. 399-407.

WOOD, I.R. (1991). "Air Entrainment in Free-Surface Flows." *IAHR Hydraulic Structures Design Manual No. 4*, Hydraulic Design Considerations, Balkema Publ., Rotterdam, The Netherlands, 149 pages.

YEH, H., LIU, P., and SYNOLAKIS, C. (1996). "Long-wave Runup Models." *World Scientific*, Singapore, 403 pages. (also *Proc. 2nd Intl Workshop on Long-Wave Runup Models*, Friday Harbour WAS, USA, Sept. 1995.)